

# Dirac-Bogoliubov-deGennes quasiparticles in a vortex lattice

Ashot Melikyan<sup>1,\*</sup> and Zlatko Tešanović<sup>2,†</sup>

<sup>1</sup>*Institute of Fundamental Theory, Department of Physics, University of Florida, Gainesville, FL, 32611*

<sup>2</sup>*Department of Physics and Astronomy, Johns Hopkins University, Baltimore, MD, 21218*

(Dated: July 2, 2018)

In the mixed state of an extreme type-II  $d$ -wave superconductor and within a broad regime of weak magnetic fields ( $H_{c1} \ll H \ll H_{c2}$ ), the low energy Bogoliubov-deGennes quasiparticles can be effectively described as Dirac fermions moving in the field of singular scalar and vector potentials. Although the effective linearized Hamiltonian operator formally does not depend on the structure of vortex cores, a singular nature of the perturbation requires choosing a self-adjoint extension of the Hamiltonian by imposing additional boundary conditions at vortex locations. Each vortex is described by a single parameter  $\theta$  that effectively represents all effects arising from the physics beyond linearization. With the value of  $\theta$  properly fixed, the resulting density of states of Dirac Hamiltonian exhibits full invariance under arbitrary singular gauge transformations applied at vortex positions. We identify the self-adjoint extensions of the solutions found earlier, within the framework of the linearized Hamiltonian diagonalized by expansion in the plane wave basis, and analyze the relation between fully self-consistent formulation of the problem and the linearized model. In particular, we construct the low-field scaling form of the nodal quasiparticle spectra which incorporates the self-adjoint extension parameter  $\theta$  explicitly and generalizes the conventional Simon-Lee scaling. In a companion paper, we also present a detailed numerical study of the lattice  $d$ -wave superconductor model and examine its low energy, low magnetic field behavior with an eye on determining the proper self-adjoint extension(s) of the linearized continuum limit. In general, we find that the density of quasiparticle states always vanishes at the chemical potential, either linearly or by virtue of a finite gap. The low energy continuum limit is thus faithfully represented by Dirac-like fermions which are either truly massless, massless at the linearized level (mass  $\sim H$ ) or massive (mass  $\sim \sqrt{H}$ ), depending on the mutual commensuration of magnetic length and lattice spacing.

PACS numbers: 74.25.Jb, 74.25.Qt

## I. INTRODUCTION

In conventional  $s$ -wave superconductors the BCS quasiparticle excitation spectrum is gapped and, in presence of a vortex defect, the quasiparticles form a discrete set of Caroli-deGennes-Matricon states<sup>1</sup>. These states are bound below the gapped continuum and are described by wavefunctions that decrease exponentially away from the vortex position. Once finite density of vortices is induced by a magnetic field, as is the case in the mixed state of type-II superconductors, these discrete levels broaden into extremely narrow quasiparticle bands whose effect on bulk properties is rather modest, as long as the magnetic field  $H$  remains well below the upper critical field  $H_{c2}$ . The situation is entirely different in high temperature cuprate superconductors: there the quasiparticle gap has a  $d_{x^2-y^2}$  symmetry and vanishes at four nodal points on the Fermi surface. The excitation spectrum is gapless, with linearly vanishing density of states at the Fermi level. As a consequence, there are no strictly bound states near a vortex defect in such a superconductor<sup>2</sup>. Instead, the quasiparticle wavefunctions exhibit a power law decrease away from vortex position and the spectrum is continuous<sup>3</sup>. Once a finite magnetic field is turned on and vortex lattice appears in the mixed state, the low energy quasiparticles are expected to form broad bands which dramatically influence thermodynamics, transport and vortex dynamics of high

temperature superconductors.

After an early semiclassical approximation due to Volovik<sup>4</sup>, who suggested that quasiparticles spectrum undergoes a Doppler shift  $E_{\mathbf{k}} \rightarrow E_{\mathbf{k}} - \mathbf{v}(\mathbf{r}) \cdot \mathbf{k}$  due to the vortex-induced superflow  $\mathbf{v}(\mathbf{r})$  at a given point  $\mathbf{r}$ , the quantum theory of quasiparticles in the presence of vortex lattice evolved along two somewhat separate lines. On one side, the self-consistent Bogoliubov-deGennes (BdG) equations for  $d$ -wave superconductor were solved numerically in continuum, both for a single vortex<sup>2</sup> and for a vortex lattice<sup>5</sup>. Additionally, the numerical solution was also obtained for BdG equations of a tight-binding lattice  $d$ -wave superconductor with boundary conditions corresponding to a periodic vortex array<sup>6</sup>. In all cases it was clearly demonstrated that a single vortex is incapable of truly localizing  $d$ -wave quasiparticles and broad low energy bands are evident in the quasiparticle excitation spectrum of a vortex lattice.

Solving BdG equations in the inhomogeneous mixed state, particularly for a  $d$ -wave superconductor with its extended low energy quasiparticle states, is a daunting task. It is natural to inquire whether a simpler, analytic description might be devised which will allow one to address important and realistic physics questions including disordered vortex lattice, thermal and quantum fluctuating vortices, etc., where numerical solutions are either too forbidding or too opaque to be useful. An important step along this path is the linearized version of the BdG

Hamiltonian introduced by Simon and Lee<sup>7</sup>. Since the homogeneous system at zero field can be described by four species of massless two-component Dirac fermions residing at nodal points on the Fermi surface, it was argued that in low magnetic fields  $H_{c1} \ll H \ll H_{c2}$ , when the separation between vortices given by magnetic length  $l$  becomes much larger than the size of the vortex cores – set by the BCS coherence length  $\xi$  – the properties of low energy quasiparticles to the leading order in  $\xi/l$  can still be described by a superposition of four independent Hamiltonians at each node<sup>7,8</sup>.

By devising an eponymous gauge transformation, Franz and Tešanović<sup>8</sup> recast the nodal BdG Hamiltonian as that of a Dirac particle moving in a zero *average* magnetic field and subject to effective long-range scalar and vector potentials whose point-like sources are located at vortex positions. This approach revealed that nodal quasiparticles couple to vortices through a *combined* effect of *two* long-range terms: the semiclassical Doppler shift must be accompanied by a purely quantum mechanical Berry phase, which attaches a  $\exp(\pm i\pi) = (-1)$  phase factor to a wavefunction of a quasiparticle encircling an  $hc/2e$  vortex<sup>8,10</sup>. The FT transformation has been widely used to directly address, by combination of general symmetry arguments<sup>9,10,12,15</sup> and explicit analytic and numerical calculations,<sup>9,10,11,13,14,15,16,17,18,19,20,21</sup> various aspects of quantum mechanics of nodal quasiparticles in presence of vortices and will serve as the departure point for our discussion<sup>22</sup>. We should stress, however, that the results and conclusions of this paper are completely general and remain unaffected if instead of the FT transformed BdG Hamiltonian one uses more familiar framework of the magnetic translations group applied to the original BdG equations. A natural question is why should not one simply use the magnetic translation group (MTG) and forgo the FT transformed problem altogether? The answer is twofold: obviously, in the FT transformed case one is dealing with representations of ordinary Bloch translation group that are far more convenient than those of MTG. More importantly, the FT transformation is custom tailored for an efficient extraction of the low-energy, long-distance sector of the original problem, a prime feature in numerous physical situations.

While the problem of *d*-wave nodal quasiparticles interacting with vortex defects is of considerable theoretical interest in itself, its rich phenomenology and relevance for numerous experiments on cuprates promote it to the forefront of modern condensed matter physics. In high temperature superconductors, the low field regime ( $H_{c1} \ll H \ll H_{c2}$ ) of the vortex state covers a large portion of the  $H - T$  phase diagram and a large body of experimental work thought to offer clues regarding microscopic origins of high temperature superconductivity is available both for analysis and future refinements. In particular, the high resolution STS/STM measurements of tunneling conductance in YBCO and BSCCO, which is proportional to the quasiparticle local density of states (LDOS), reveal peaks near vortices

that appear at energies 5.5 meV in YBCO and 7 meV in BSCCO and at magnetic fields  $\sim 6$  Tesla<sup>23</sup>. The origin of the LDOS peaks is still a hotly debated subject and several scenarios<sup>2,24,25,26,27,28,29,30,31,32,33,34,35,36,37,38,39,40</sup> describing various microscopic physics inside and around vortex cores, such as spin- and charge- density waves (SDW and CDW), Mott insulator, *d*-density wave and others, have been proposed to explain these features. This structure in the quasiparticle LDOS appears related to the experiments on neutron scattering<sup>44</sup> which hint at the development of an antiferromagnetic order parameter localized in the vicinity of vortex cores. A mean-field factorization of  $t - J$  model on a tight-binding lattice and allowing for both *d*-wave superconductor and AF orders does indeed, for a certain range of parameters in the self-consistent solution, describe a *d*-wave vortex state with an AF order developing inside vortex cores<sup>24,25,30,36,39</sup>. The details of the calculations, however, depend strongly on the parameters of the model and the actual pairing terms included in self-consistent approximation. In fact it is not even clear that the interior of vortices can be reliably described within the mean-field framework since the suppression of superconductivity inside vortices is likely to lead to a formation of a strongly correlated state characteristic of the pseudogap region in the phase diagram of cuprates<sup>26,38,40</sup>.

The linearized continuum formulation of the bulk properties of nodal quasiparticles has the distinct advantage of being essentially independent of such details pertaining to the structure near vortex cores. Nodal BdG quasiparticle behaves like a massless Dirac fermion and can be thought of as “critical”<sup>41</sup>: the Feynman path integral trajectories of such particles lack any characteristic lengthscale. This “criticality” implies a certain degree of “universality”<sup>42,43</sup>: one expects that an effective low-energy theory of such Dirac fermions can be constructed, which incorporates all the effects of intra-vortex physics on the bulk properties of the BdG quasiparticles in terms of few simple parameters. A detailed derivation of such an effective theory, describing the influence of the physics in vicinity of vortex cores on properties of nodal BdG quasiparticles in the bulk, is the main goal of this paper.

Following FT, we start by representing the motion of nodal BdG quasiparticles in a vortex lattice by massless two-dimensional Dirac fermions in combined vector and scalar potentials<sup>8</sup>. Both vector and scalar potentials are singular near vortices, and we will show that regularization of this singular behavior is required, which itself depends on the short-scale features of the physics near vortex cores. The final effective theory is essentially the canonical FT Hamiltonian supplemented by a boundary condition at each vortex. The variety of possible physical scenarios describing different types of core and near-core behaviors is represented by a *single* dimensionless parameter  $\theta \in [0, \pi)$  that characterizes the boundary condition and is associated with each vortex.  $\theta$  being dimensionless, such boundary conditions can in principle modify the energy spectrum already at the leading or-

der in  $(k_F l)^{-1}$  – to this order<sup>45</sup> the value of  $\theta$  uniquely determines the full extent of the influence that the structure in or near vortex cores has on the bulk properties of nodal quasiparticles<sup>46</sup>. We generalize the conventional Simon-Lee scaling to include the explicit dependence on  $\theta$  and numerically determine the scaling function. This generalized scaling form for the linearized quasiparticle energy levels is:

$$E_{n,\mathbf{k}} = \frac{\hbar v_F}{l} \mathcal{E}_{n,\mathbf{k}l} \left( \frac{v_F}{v_\Delta}, \{\theta\} \right), \quad (1)$$

where  $\mathcal{E}$  is a universal dimensionless function,  $n$  and  $\mathbf{k}$  denote the band number and the Bloch momentum of the FT transformed states, respectively and  $v_F/v_\Delta$  is the bare anisotropy of the  $d$ -wave nodes in a zero-field case.

We find three prominent behaviors of a  $d$ -wave superconductor as  $H \rightarrow 0$  (while still  $H \gg H_{c1}$ ) and determine the associated self-adjoint extensions of the linearized continuum problem: the first is a gapless behavior with the Dirac nodes intact – although renormalized by the field – but with their number *doubled* relative to the zero field result of four. This solution bears considerable resemblance to the one reported earlier in Ref. 8. Second, we find new *gapped* spectra with no zero energy states. This self-adjoint extension produces a Dirac mass gap which scales as  $1/l$  and is thus a part of the leading order  $H \rightarrow 0$  scaling function, unlike the gaps of order  $1/l^2$ , which vanish in the leading order scaling and are typically present even for the “gapless” case. The gapped solution seems to be related to the “interference” gapped spectra discussed in Refs. 10,47. Finally, we find  $\theta$  for which the quasiparticle bands lack  $(E, \mathbf{k}) \rightarrow (-E, \mathbf{k})$  symmetry and for which the density of states is finite at the Fermi level – such solutions, however, at least for the superconducting gap parameter  $\Delta$  not exceedingly small in comparison to hopping  $t$ , as is appropriate for near optimally doped or underdoped cuprates, are never found in our numerical calculations on the lattice  $d$ -wave superconductor. These tight-binding calculations, reported separately<sup>47</sup>, always find either a linearly vanishing or gapped density of states at the Fermi level. Thus, the so-called “Volovik effect,” a defining feature of an early semiclassical approach, is effectively absent from a fully quantum mechanical solution. It would be important to verify this feature of our results experimentally, for example, by precision measurements of a specific heat or thermal conductivity.

Alternatively, the above regularization and associated self-adjoint extensions can be implemented by introducing a fictitious potential which suppresses the wavefunctions of nodal quasiparticles near vortices. This potential represents the nonlinear corrections to the linearized BdG Hamiltonian. Because of the well-known Klein paradox for Dirac particles, this potential cannot be chosen as a large scalar potential barrier, and instead must be realized as a position-dependent mass<sup>48</sup>, which grows rapidly as one approaches a vortex location but vanishes elsewhere. We demonstrate that the two descriptions of the regularized FT Hamiltonians are equiv-

alent and yield essentially identical results in numerical calculations. The realization that the boundary condi-

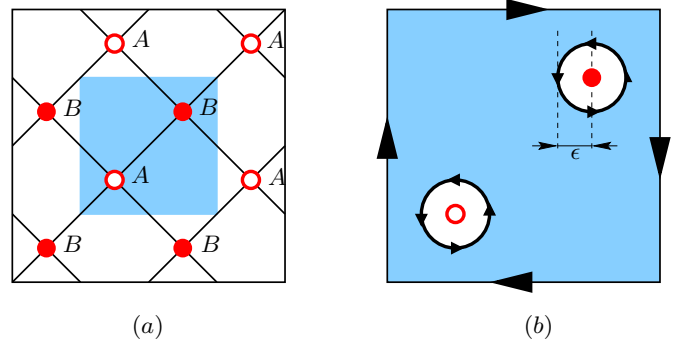


FIG. 1: A magnetic unit cell containing two vortices. Panel (b) shows contours used in the application of the Stokes theorem discussed in section III.

tions at the vortices must be externally imposed resolves the difficulty associated with previous attempts to find the spectrum of the quasiparticles numerically. Despite the gauge invariance of the linearized problem, the explicit form of the FT Hamiltonian depends on the partition of the original vortex lattice into two sublattices A and B. Such choice is clearly not unique, and different selections are related by singular gauge transformations. Obviously, all measurable physical quantities, exemplified by the density of states (DOS), must be invariant under such transformations. Surprisingly, numerical spectra of the linearized FT Hamiltonian exhibit small but persistent difference for distinct choices of A and B sublattices, when the wavefunctions are sought as linear combinations of plane waves<sup>10</sup> or when the Hamiltonian is solved by discretization on a real space mesh<sup>9,49</sup>. In what follows, we will demonstrate that the difficulties associated with the linearized model indeed are not simply a nuisance related to the numerical procedure but rather reflect a genuine dependence of the bulk properties of quasiparticles on the internal structure of vortices. Even though the bulk of 2D CuO planes is dominated by pure nodal  $d$ -wave quasiparticles, the internal vortex structure affects the spectrum through boundary conditions that should be imposed at the vortex locations, due to singular nature of the perturbation introduced by vortices, and the resulting energy spectra for different vortex core types are generally distinct to the leading order in  $\hbar v_F/l$ . We reanalyze the solutions found earlier, and find that they correspond to mutually different sets of boundary conditions, “spontaneously” selected by a numerical procedure used as well as the choice of A and B sublattices. Once the fixed boundary conditions are externally imposed, the numerical procedure that incorporates them generates results that are fully gauge independent.

The paper is organized as follows: in the next two sections we introduce the linearized FT Hamiltonian and discuss the necessity of imposing boundary conditions (BC) at vortex locations. We show how these BC are intimately related to the self-adjoint extensions of the lin-

earized BdG Hamiltonian<sup>10</sup> and discuss such extensions in detail in section III. After analyzing the symmetry properties of the linearized problem with and without BC in section IV, we describe in section V a new procedure used to address the problem, which incorporates the BC numerically. Section VI establishes an alternative framework for regularization of the linearized problem using mass potentials and discusses the connection between the full, non-linearized BdG equations and self-adjoint extensions of the linearized model. This is followed by a general discussion of the relation between the  $d_{xy}$  and  $d_{x^2-y^2}$  continuum models in section VII. Finally, we conclude with a brief summary of our results.

## II. THE LINEARIZED HAMILTONIAN

It was argued<sup>7,8</sup> that in the limit of weak magnetic field  $H \ll H_{c2}$  (but still  $H \gg H_{c1}$ ), the BdG Hamiltonian describing quasiparticles in an ideal vortex lattice can be formally expanded<sup>22</sup> in powers of  $(k_F l)^{-1}$  where magnetic length  $l$  is defined through the flux quantum  $\Phi_0 = hc/e$  as  $l = \sqrt{\Phi_0/H}$ . In extreme type-II superconductors, the regions separated from the vortices by distances sufficiently larger than vortex core size  $\sim \xi$  are accurately described by the center-of-mass superconducting order parameter  $\Delta(\mathbf{r}) = \Delta_0 e^{i\phi(\mathbf{r})}$  with a nearly uniform amplitude  $\Delta_0$ . One can then avoid solving the full self-consistent problem by eliminating the effective coupling constant in favor of  $\Delta_0$ . In making this useful simplification, one implicitly excludes small disks of radius  $\sim \xi$  around each vortex in a 2D plane, where the amplitude of the order parameter varies appreciably. This amounts to a tacit assumption that, in the limit  $\xi \ll l$ , the effects of the detailed structure around vortex cores on properties of the far-away nodal states in the bulk regions are entirely negligible. It is this assumption that needs to be revisited, as we will show. Initially, however, we will follow this assumption in order to understand the difficulties it generates and to introduce the notation.

One starts from the BdG Hamiltonian for a  $d$ -wave extreme type-II superconductor:

$$\mathcal{H}_{BdG} = \begin{pmatrix} \frac{(\mathbf{p} - \frac{e}{c}\mathbf{A})^2}{2m} - \epsilon_F & \hat{\Delta} \\ \hat{\Delta}^* & \epsilon_F - \frac{(\mathbf{p} + \frac{e}{c}\mathbf{A})^2}{2m} \end{pmatrix}. \quad (2)$$

The gap operator  $\hat{\Delta}$  is given by<sup>10</sup>

$$\hat{\Delta} = \frac{1}{\hbar^2 k_F^2} \{p_x, \{p_y, \Delta(\mathbf{r})\}\} - \frac{i}{4k_F^2} \Delta(\mathbf{r}) (\{\partial_x, \partial_y\} \phi), \quad (3)$$

where  $\Delta(\mathbf{r})$  is the superconducting center-of-mass complex gap function,  $\phi$  is its phase and curly brackets denote anticommutation operator  $\{a, b\} = (ab + ba)/2$ , accompanied by the  $x \leftrightarrow y$  symmetrization. Note that the first term<sup>7</sup> in Eq. (3) must be accompanied by the second<sup>8,10</sup> to maintain gauge invariance of the BdG Hamiltonian – this amounts to replacing ordinary derivatives in the first

term by the covariant ones:  $\nabla \rightarrow \nabla + (i/2)(\nabla\phi)$ , insuring minimal coupling of  $\phi$  to the external electromagnetic gauge potential, with charge equal to  $2e$ . Although the gap operator  $\hat{\Delta}$  in the above form has a  $d_{xy}$  symmetry, the results for  $d_{x^2-y^2}$  can be readily obtained after a simple rotation by  $\pi/4$ .

In a uniform external magnetic field  $H$  and in the presence of a periodic array of superconducting vortices which the field induces in  $\Delta(\mathbf{r})$ , both diagonal terms and the gap operator in (2) are invariant under *magnetic* translation group transformations (MTG) rather than being simply periodic in space. Consequently, the eigenfunctions of  $\mathcal{H}_{BdG}$  are not the ordinary Bloch functions but are instead the so-called *magnetic* Bloch functions and can be classified according to representations of MTG<sup>50,51,52</sup>. An essential aspect of the problem is the observation that a simple Bravais lattice of superconducting vortices contains a magnetic flux equal to  $hc/2e$  per unit cell – this is just a reflection of the fact that a vortex is a topological defect in the phase of the gap function of Cooper pairs which carry charge  $2e$ . In contrast, all representations of MTG in terms of single-valued eigenfunctions must contain an integer number of the *electronic* flux quanta,  $hc/e$ , per unit cell. It is therefore necessary to choose the unit cell of the MTG so it is at least twice as large as that of the vortex lattice<sup>53,54</sup>. Apart from this condition the shape and the size of such unit cell are arbitrary and different choices correspond to different “gauges”, i.e. different representations of MTG. The eigenfunctions associated with these representations are different but the spectrum of eigenvalues of  $\mathcal{H}_{BdG}$ , as measured by its density of states, is the same for all these choices of MTG.

FT observed that the above features of MTG can be used to recast the original problem in a more convenient form. One first partitions the original vortex lattice into two sublattices A, B (Fig. 1) and then performs a singular gauge transformation  $\mathcal{H}' = U^{-1}\mathcal{H}U$ :

$$U = \begin{pmatrix} e^{i\phi_A} & 0 \\ 0 & e^{-i\phi_B} \end{pmatrix}, \quad \phi(\mathbf{r}) = \phi_A(\mathbf{r}) + \phi_B(\mathbf{r}), \quad (4)$$

where  $\phi_{A(B)}$  are contributions to the phase of the order parameter from vortices of A(B) sublattice (see<sup>55</sup> and Appendix A). After the transformation the Hamiltonian assumes a periodic form:

$$\mathcal{H} = \begin{pmatrix} \frac{(\mathbf{p} + m\mathbf{v}_A)^2}{2m} - \epsilon_F & \hat{D} \\ \hat{D} & \epsilon_F - \frac{(\mathbf{p} - m\mathbf{v}_B)^2}{2m} \end{pmatrix}, \quad (5)$$

where the transformed gap operator is given by

$$\hat{D} = e^{-i\phi_B} \hat{\Delta} e^{i\phi_A} = \frac{\Delta_0}{\hbar^2 k_F^2} \{p_x + a_x, p_y + a_y\} \quad (6)$$

and two superfluid velocities are defined as

$$m\mathbf{v}_{A,B}(\mathbf{r}) = \hbar\nabla\phi_{A,B}(\mathbf{r}) - e\mathbf{A}/c, \quad (7)$$

$$\mathbf{a} = (m\mathbf{v}_A - m\mathbf{v}_B)/2. \quad (8)$$

Properties of the superfluid velocities  $\mathbf{v}_A$  and  $\mathbf{v}_B$  are discussed at length further in the text and in the Appendix. The crucial feature is that their chirality, set by  $\nabla \times \mathbf{v}_{A(B)}(\mathbf{r})$ , vanishes on *average* and thus  $\mathbf{v}_{A(B)}$  are truly periodic functions in space. Consequently, the eigenstates of the FT transformed BdG Hamiltonian are ordinary Bloch waves that can be classified by their crystal momentum and band index. In the limit of weak fields it is reasonable to view the low energy wavefunctions as “perturbations” of the nodal states at  $H = 0$ , and therefore the wavefunctions describing states close to the nodal point  $\mathbf{k}_1^F = (k_F, 0)$  can be described as

$$\Psi(\mathbf{r}) = e^{ik_F x} \psi(\mathbf{r}),$$

where  $\psi_1(\mathbf{r})$  changes weakly on distances of order  $1/k_F$ . Under assumptions  $|\nabla\psi(\mathbf{r})| \ll k_F|\psi(\mathbf{r})|$ ,  $m\mathbf{v}(\mathbf{r}) \ll \hbar k_F$ , and  $\hbar\nabla^2\psi \ll k_F|m\mathbf{v}(\mathbf{r})|$ , the Hamiltonian to the leading order is<sup>8</sup>

$$\mathcal{H}_{FT} = v_F(p_x + a_x)\sigma_3 + v_\Delta\sigma_1(p_y + a_y) + mv_Fv_x, \quad (9)$$

where  $\sigma_i$  are the standard Pauli matrices and  $\mathbf{v} = (\mathbf{v}_A + \mathbf{v}_B)/2$  is the gauge invariant superfluid velocity. The corrections to (9) fall into two categories: more familiar ones, of higher order in  $(k_F l)^{-1} \ll 1$  become arbitrarily small as  $H \rightarrow 0$ . In addition, however, there are corrections governed by  $(k_F \xi)^{-1} \ll 1$  even as  $H \rightarrow 0$ , which reflect the fact that nodes are located at *finite* momentum  $k_F$  and describe rapid oscillations in quasiparticle spectra due to internodal interference<sup>10,46,47</sup>.

The linearized Hamiltonian  $\mathcal{H}_{FT}$  describes a massless Dirac particle with anisotropic dispersion in presence of an internal gauge field  $\mathbf{a}(\mathbf{r})$  and a scalar potential  $v_x$  given by the component of  $\mathbf{v}(\mathbf{r})$  along the node. This scalar potential is nothing but the Doppler shift of nodal quasiparticle energies in the superflow field produced by vortices. The internal gauge field  $\mathbf{a}(\mathbf{r})$  – its minimal coupling to BdG quasiparticles betraying its topological origin – corresponds to an array of  $\pm\frac{1}{2}$  Aharonov-Bohm fluxes located at vortex positions and generates the required  $\pm\pi$  Berry phases for fermions circling around vortices<sup>8,10,56</sup>. This intrinsic topological frustration is entirely absent in semiclassical approximations<sup>4</sup> but plays an essential role in the quantum mechanics of nodal quasiparticles in presence of vortices. Note that  $\mathbf{a}(\mathbf{r})$  is explicitly time-reversal invariant since the Aharonov-Bohm effect remains unaffected by the exchange of direction of a half-flux. This is an important feature and the necessary condition for invariance of physical results under different FT gauge transformations. Different FT transformations correspond to different choices of A and B sublattices (always, however, containing the same total number of vortices so that  $\nabla \times \mathbf{v}_{A(B)}(\mathbf{r})$  remains zero on average) closely resembling different choices of the unit cell of the MTG. Under such transformations the Hamiltonian (9) retains its general form but with half-fluxes in  $\mathbf{a}(\mathbf{r})$  switching their signs from positive to negative depending on whether they belong to A or B sublattice, while  $\mathbf{v}(\mathbf{r})$  remains the same in all FT gauges.

Hamiltonian  $H_{FT}$  is periodic and has a well defined Fourier representation. While the fact that both effective potentials  $\mathbf{a}(\mathbf{r})$  and  $\mathbf{v}(\mathbf{r})$  diverge as  $1/r$  near vortices is an obvious point of concern, resulting in matrix elements of perturbation theory that decrease only as  $1/k$  in momentum space, one still reasonably expects that the path toward finding the set of eigenfunctions of  $H_{FT}$  starts by simply expanding them in a plane wave basis. The numerical solution obtained in this manner,

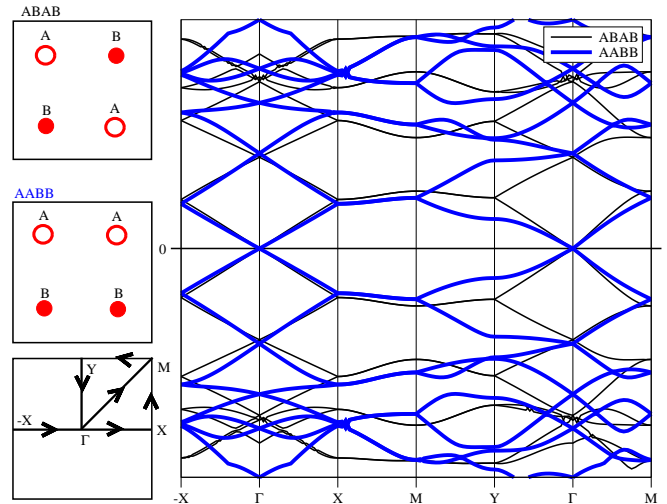


FIG. 2: Comparison of energy spectra for different choices of A and B sublattices. The spectra are similar at low energies but differ significantly as energy increases<sup>57</sup>. Lower left: the first magnetic Brillouin zone.

shown in Fig. 5, was found to result in strongly dispersive bands at low energies. The low-energy portion of the spectrum appears qualitatively similar to the zero-field case and, most importantly, preserves nodal point:  $\epsilon(\mathbf{k}) = \hbar\sqrt{v_F^2 k_x^2 + v_\Delta^2 k_y^2}$ . The only significant effect of finite field is the renormalization of the original velocities  $v_F$  and  $v_\Delta$ . The band structure calculation was also confirmed in<sup>9</sup>, where the spectrum and the eigenstates of  $H_{FT}$  (9) were obtained by discretization of the Hamiltonian in real space. The persistence of nodal points was further demonstrated<sup>9,12</sup> to be a consequence of the general symmetry properties of  $H_{FT}$ .

As noted previously<sup>10</sup>, the choice of A-B sublattice arrangement is not unique in the FT transformation, being merely a choice of singular gauge. Clearly, measurable quantities such as the density of states (DOS) should not depend on the partitioning of vortex lattice into various A and B sublattices. On the other hand, the Hamiltonian  $H_{FT}$  has a formal dependence on the FT singular gauge choice, and surprisingly, the numerical solution exhibits small but persistent differences for different arrangements of A and B sublattices (Fig. 2). The discrepancy remains regardless of whether the computation is done by expanding the solution in plane wave basis<sup>8,10</sup> or by discretization in real space<sup>9</sup>. Note that these difficulties *cannot* simply be attributed to the singular na-

ture of the FT gauge transformation: the energy spectrum of the Hamiltonian in the *original* representation, where the eigenfunctions are chosen as magnetic translation group eigenstates, has DOS which also exhibits a similar discrepancy for different choices of a magnetic unit cell (e.g. rectangular vs. square). As a remedy, the tight-binding formulation of a  $d$ -wave BdG Hamiltonian and FT transformation was introduced in<sup>10</sup>, where it was verified that this so-called “ABAB vs. AABB” problem does not appear and the spectra are explicitly invariant under singular gauge transformations for arbitrary size of the tight-binding mesh. In a way, this is the resolution of the whole “ABAB vs. AABB” problem: CuO<sub>2</sub> planes in high temperature superconductors are actually well described by an effective tight-binding Hamiltonian (of a  $t-J$ , Hubbard or a related variety) and the lattice  $d$ -wave superconductor and its BdG equations is precisely what we should be considering. The problem with the singular  $1/r$  behavior never arises since BdG quasiparticles live on sites while vortices are “located” in the interior of plaquettes of a tight-binding lattice.

Nevertheless, the appeal of the continuum formulation is undeniable. By representing nodal quasiparticles as massless Dirac fermions one is hoping that their interactions with vortices can be described by a relatively simple and elegant effective continuum theory which can then become the starting point for analytic exploration of more complex problems involving fluctuating or disordered vortices, thermal and quantum fluctuations of vortex-antivortex pairs, etc. It is therefore highly desirable to understand the source of difficulties besetting the continuum description of the linearized model and to overcome them<sup>58</sup>. Moreover, as pointed in the Introduction, a detailed structure of vortex cores in cuprates is unknown at present and all possible tight-binding approaches will necessarily suffer from being dependent on short-range physics details, which, as one suspects, should have only a limited effect on the nodal quasiparticle wavefunctions in the bulk and thus on any effective low-energy theory. The linearized theory, in contrast, is formulated in terms of a universal Hamiltonian (9), which is completely independent of short-range details, including the structure of vortex cores.

### III. SELF-ADJOINT EXTENSIONS

The origin of the difficulties with different choices of FT singular gauge can be traced back to the assumptions made during the linearization procedure outlined above Eq. (9). Although the conditions necessary for linearization are well satisfied for weak magnetic fields and in the bulk, far away from vortex cores ( $r \sim l$ ), they are violated at distances  $r \sim \xi$ , since the neglected terms diverge as  $1/r^2$  near vortices. Thus one suspects that additional regularization might be required to take into account the effect of such terms. Let us nevertheless assume for a moment that the dependence on A-B ar-

rangement *is* caused by a numerical procedure. Since the scalar and vector potentials  $\mathbf{a}(\mathbf{r})$  and  $\mathbf{v}(\mathbf{r})$  diverge as  $1/r$  as one approaches a vortex, one naturally expects that by finding the asymptotic behavior of the eigenfunction near vortices, one can use it to his/her advantage to cure the singularities. The asymptotics in fact were found analytically by Melnikov<sup>59</sup>. For brevity, in this article we will consider mostly the isotropic case ( $v_F = v_\Delta$ ); the results are easily generalized to the anisotropic case.

Close to a vortex two linearly independent solutions of the eigenvalue problem for the linearized Hamiltonian  $\mathcal{H}_{FT}$  are described by the wavefunctions that diverge near the vortex as  $r^{-1/2}$ . The angular dependence of the divergent part of the wavefunctions  $\sqrt{r}\psi(\mathbf{R}_A + \mathbf{r})$  near vortex A is described by

$$C_1 e^{\frac{i \cos \varphi}{2}} \begin{pmatrix} e^{-i\varphi} - i \\ ie^{-i\varphi} - 1 \end{pmatrix} + C_2 e^{-\frac{i \cos \varphi}{2}} \begin{pmatrix} e^{-i\varphi} + i \\ ie^{-i\varphi} + 1 \end{pmatrix}, \quad (10)$$

where  $\varphi$  (not to be confused with  $\phi(\mathbf{r})$ , the phase of the gap function) is the polar angle around a particular vortex. The above is only the dominant part of each eigenfunction as  $r \rightarrow 0$ ; the prefactors of this diverging term as well as subdominant terms are different for different eigenfunctions. Generally, the weight of the divergent term in an eigenfunction decreases as its energy eigenvalue increases. The angular dependence of the singular part of the wavefunctions near vortices of B sublattice  $\sqrt{r}\psi(\mathbf{R}_B + \mathbf{r})$  is given by an expression similar to (10):

$$C'_1 e^{\frac{i \cos \varphi}{2}} \begin{pmatrix} 1 - ie^{i\varphi} \\ i - 1e^{i\varphi} \end{pmatrix} + C'_2 e^{-\frac{i \cos \varphi}{2}} \begin{pmatrix} 1 + ie^{i\varphi} \\ i + 1e^{i\varphi} \end{pmatrix}. \quad (11)$$

The asymptotics above can be checked by retaining only the divergent parts of the potentials  $\mathbf{v}$  and  $\mathbf{a}$  in the FT equations with the radial dependence proportional to  $1/r$ . Such “zeroth-order” approximation describes a single vortex, since both the superfluid velocity and the vector potential can be represented as a sum (see Eq. (A9) of the Appendix). Each term of the sum represents contribution of an individual vortex, and by neglecting all terms of the sum that are finite only the contribution of a single vortex is taken into account. Then, one can easily verify that (10) or (11), for a vortex belonging to class A or B respectively, are exact eigenfunctions corresponding to zero energy. Returning now to the lattice problem, the non-singular part of the Hamiltonian,  $\hat{V}_{reg}$ , which is due to other vortices, can be treated as a perturbation. Such finite terms do not modify the limiting small  $r$  behavior of the zero energy eigenstates (if there are any). Moreover, under the action of perturbation  $V_{reg}$ , the nonzero energy eigenstates are mixed with the singular wavefunctions (10) or (11), and therefore are described by the same limiting behavior close to any particular vortex.

The eigenfunctions of  $\mathcal{H}_{FT}$  obtained numerically by the plane wave expansion close to a vortex will be shown below (see Fig. 3) to have asymptotic behavior given by either (10) or (11) for vortices belonging to sublattice A or B, respectively. Additionally, the increase of

the wavefunctions according to power law  $r^{-1/2}$  and angular dependence given above near vortices at distances  $\xi \ll r \ll l$  has been explicitly verified<sup>60</sup> for the solutions of BdG equations describing the tight-binding lattice  $d$ -wave superconductor<sup>10,65</sup>.

Note that Eq. (10) describes *two linearly independent* solutions *both* of which diverge as  $1/\sqrt{r}$  as one approaches the vortex. For non-singular potentials only one of the solutions would have been square-integrable, and the second solution would have to be discarded. Thus, before one proceeds, one must decide whether such divergent solutions are permitted in the spectrum.

### A. Dirac particles in the field of Aharonov-Bohm flux

This issue is not entirely new, and similar problems were encountered in the context of cosmic strings<sup>61</sup>. There, a Dirac particle is considered in the field of a single Dirac string carrying a fractional magnetic flux. We will restrict our discussion to the relevant case of a single half-integer flux:

$$\begin{pmatrix} p_x + a_x & p_y + a_y \\ p_y + a_y & -p_x - a_x \end{pmatrix} \begin{pmatrix} u \\ v \end{pmatrix} = E \begin{pmatrix} u \\ v \end{pmatrix}, \quad (12)$$

where  $\mathbf{a} = \frac{(-y, x)}{2r^2}$  is the vector potential corresponding to the Aharonov-Bohm half-flux. The Hamiltonian can be obtained from (9) where the last term describing scalar potential is set to zero. After rotation  $\chi_1 = u - iv$ ,  $\chi_2 = u + iv$  we obtain Hamiltonian in the basis used in 61:

$$H_{GJ} = \begin{pmatrix} 0 & p_x + a_x - i(p_y + a_y) \\ p_x + a_x + i(p_y + a_y) & 0 \end{pmatrix}. \quad (13)$$

The eigenstates of  $H_{GJ}$  can be expressed through Bessel functions as

$$\begin{pmatrix} \chi_1 \\ \chi_2 \end{pmatrix} = e^{in\varphi} \left[ C_1 \begin{pmatrix} J_{n+1/2} \\ ie^{i\varphi} J_{n+3/2} \end{pmatrix} + C_2 \begin{pmatrix} J_{-n-1/2} \\ -ie^{i\varphi} J_{-n-3/2} \end{pmatrix} \right]. \quad (14)$$

Gerbert and Jackiw noticed that for all angular channels except  $n = -1$  the square integrability requirement specifies which of the two independent solutions in (14) should be present. For  $n = -1$ , however, there is an ambiguity as both solutions are square integrable, but divergent as  $1/\sqrt{r}$  at the origin. They found that keeping both wavefunctions in the spectrum results in an overcomplete basis, with such pathologies as imaginary eigenvalues of the Hamiltonian. On the other hand, the requirement of continuity (non-divergence) of the wavefunctions at the origin is too strong and causes the loss of completeness in the angular momentum channel.

The complications are due to the singular nature of the vector potential  $\mathbf{a}(\mathbf{r})$  at the origin. The usual spectral theorems, normally derived for *bounded* symmetric (Hermitian) operators, do not hold automatically for singular

potentials and a more careful analysis is needed. The domain of finite wavefunctions should be enlarged to include a specific linear combination of  $1/\sqrt{r}$ -divergent solutions. Using the language of functional analysis, self-adjoint extensions of the Hamiltonian should be constructed<sup>63</sup>. Gerbert and Jackiw found that the mathematically allowed linear combination of divergent wavefunctions is not unique but forms a one-parameter family

$$\begin{aligned} \chi \propto \sin \theta \begin{pmatrix} J_{-1/2}(Er) \\ ie^{i\varphi} J_{1/2}(Er) \end{pmatrix} + \cos \theta \begin{pmatrix} J_{1/2}(Er) \\ -ie^{i\varphi} J_{-1/2}(Er) \end{pmatrix} \\ \sim \frac{1}{\sqrt{r}} \begin{pmatrix} \sin \theta \\ -ie^{i\varphi} \cos \theta \end{pmatrix}, \quad (15) \end{aligned}$$

where  $\theta \in [0, \pi)$  is a real parameter that labels distinct self-adjoint extensions. The parameter  $\theta$  expressing the boundary condition cannot be found from the model that treats the string as a “black box”; it depends on the short-scale structure of the string.

A string described by a divergent vector potential at  $r = 0$  is of course only an idealization. To find appropriate  $\theta$  one has to consider the physical regularization of the problem. The simplest case of magnetic field concentrated in a thin cylindrical shell of small, but finite radius  $\epsilon$  when  $\epsilon \rightarrow 0$  was considered in 64. By matching solutions inside and outside the core, the authors found that for radially extended symmetrical distribution of magnetic field inside the core one obtains  $\theta = 0$ , implying that the lower component of spinor  $\chi$  stays regular at the origin. The procedure can be repeated for physical, extended fluxes carrying arbitrary half-integer flux  $\Phi$ , and it was found that for  $\Phi = 1/2, 3/2, 5/2, 7/2, \dots$  the self-adjoint extension is the same  $\theta = 0$  and the solutions for positive half-integer fluxes are related to each other by singular gauge transformations  $\chi(\mathbf{r}) \rightarrow \exp(iN\varphi)\chi(\mathbf{r})$ . Quite surprisingly, the negative extended half-integer fluxes  $\Phi = -1/2, -3/2, \dots$  belong to a different class  $\theta = \pi/2$  which corresponds to wavefunctions with regular upper components of  $\chi$ . Thus, the symmetry  $\Phi \rightarrow \Phi + 1$  is broken around  $\Phi = 0$ . Due to the unbounded increase of the wavefunctions, a relativistic fermion can “probe” the short-scale structure of the core and the direction of the flux is “exported” to the exterior through boundary condition<sup>64</sup>. Although physical, extended fluxes do have different limiting solutions for opposite orientations of magnetic field as the size of the core is taken to zero, one can still perform singular gauge transformations, of course, provided that the boundary condition  $\theta$  is chosen correctly to reflect the direction of the real, physical magnetic field.

A necessity of considering self-adjoint extensions is not restricted to a single-flux problem. In the case of two fluxes the problem can also be solved essentially exactly; the solution is presented in the Appendix B.

## B. Dirac particle in the field of periodic array of singular scatterers

The above analysis of a single flux problem<sup>61</sup> is facilitated due to the knowledge of exact eigenfunctions allowing for application of the von Neumann theorem on self-adjoint extensions<sup>63</sup>. To consider an array of vortices, we will rederive the result (15) by following a different procedure, which will allow us to find the self-adjoint extensions corresponding to the vortex lattice problem, for which exact eigenfunctions are unknown. We consider a general Hamiltonian

$$H = \begin{pmatrix} p_x + V_{11} & p_y + V_{12} \\ p_y + V_{21} & -p_x + V_{22} \end{pmatrix}, \quad (16)$$

where  $V_{ij}$  are arbitrary periodic functions which can diverge at most as  $1/r$  at a certain finite set of points in unit cell, such as positions of fluxes or vortices.

In order for Hamiltonian (9) to be a symmetric operator  $(\psi^* H \chi) = (\chi^* H \psi)^*$ , the condition

$$\int [\partial_x(\chi_1 \psi_1^* - \chi_2 \psi_2^*) + \partial_y(\chi_1 \psi_2^* + \chi_2 \psi_1^*)] d^2 r = 0 \quad (17)$$

must be fulfilled. This is satisfied automatically if  $\chi(\mathbf{r})$  and  $\psi(\mathbf{r})$  have different crystal momenta, and therefore we concentrate on the subspace of the wavefunctions with the same crystal momentum  $\mathbf{k}$ , but different band indices. Symmetric operator is self-adjoint if the domain  $D(H)$  coincides with that of its adjoint  $D(H^*)$ . In other words, we have to find such a boundary condition on  $\psi(\mathbf{r})$  so that the adjoint wavefunctions  $\chi(\mathbf{r})$  satisfy precisely the same condition. For the subspace of functions characterized by the same crystal momentum  $\mathbf{k}$ , the integrand of (17) is periodic in space, and therefore the integral over entire space can be replaced by an integral over one unit cell. It may appear that the integral automatically vanishes; by Stokes theorem it can be transformed into a contour integral along the edges of the unit cell, which in turn vanishes due to the periodicity of the integrand. Indeed, this conclusion is valid for *regular* wavefunctions. It must be remembered, however, that the necessary condition for Stokes theorem to hold is the continuity of the partial derivatives in the integrand in (17) inside the contour, and in our case, with  $\psi \propto 1/\sqrt{r}$  near a vortex, the theorem does not automatically apply. To proceed with the analysis, we define

$$\begin{cases} \mathcal{A}_x = \chi_1 \psi_2^* + \chi_2 \psi_1^* \\ \mathcal{A}_y = \chi_2 \psi_2^* - \chi_1 \psi_1^* \end{cases} \quad (18)$$

and separate the contribution of singularities near the vortices by drawing discs  $\Gamma_i$  of radii  $\epsilon_i$  surrounding each vortex (see Fig. 1(b) for the case of two vortices per unit cell).

After Stokes theorem is applied to the exterior of the discs within the unit cell, where the wavefunctions are finite, the contribution from the edges cancels by periodicity, and we find that the sum of the contour integrals

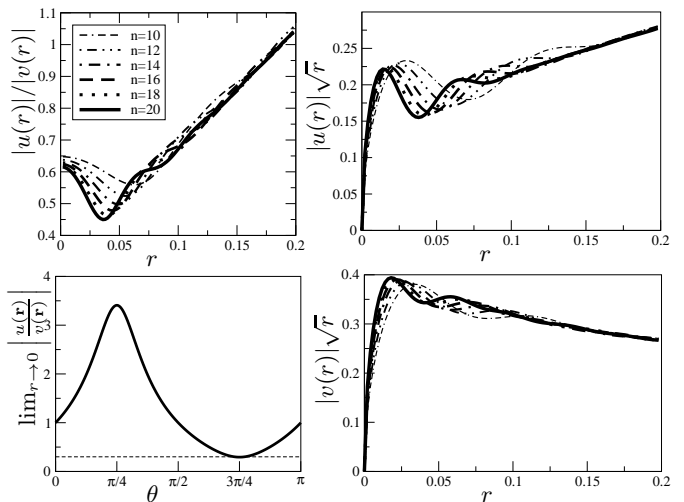


FIG. 3: Typical eigenfunctions of the linearized equation found by expanding the wavefunctions in plane wave basis without explicitly imposing boundary conditions at vortex locations.  $N = (2n + 1)^2$  plane waves are included in numerical solution. Right panels:  $\sqrt{r}|u(r)|$  and  $\sqrt{r}|v(r)|$  along fixed direction  $\varphi = 0$  as functions of distance from the vortex. Each plot approaches a straight line as the accuracy is increased. The convergence is non-uniform exhibiting Gibbs overshoot as expected, because of the singularity of the wavefunction at the origin. Upper left panel: ratio  $|u(r)/v(r)|$  used to extract  $\theta$ . The intercept of the limiting linear dependence ( $0.3+0.67r$ ) is used to find  $\theta$  as shown in the lower left panel.

along the boundaries of the discs  $\Gamma_i$  and the area integrals over the interior of  $\Gamma_i$  equals

$$\sum_i \int_0^{2\pi} (\sin \varphi A_y(\epsilon_i, \varphi) - \cos \varphi A_x(\epsilon_i, \varphi)) d\varphi = 0, \quad (19)$$

where  $i$  labels the vortices in unit cell and  $\varphi$  is the polar angle around the  $i$ th vortex. Obviously, if one demands that  $\psi(\mathbf{r})$  are regular at the origin, then the adjoint domain of  $\chi$  includes all solutions that behave as  $1/\sqrt{r}$ , leading to  $D(H) \neq D(H^*)$ . Now note that in the limit  $\epsilon_i \rightarrow 0$  only the singular part of the wavefunctions (10) and (11) contributes. Since the limits  $\epsilon_i \rightarrow 0$  can be taken independently, it is straightforward to find from (19) that the self-adjointness requirement  $D(H) = D(H^*)$  fixes the relative phase between two asymptotic solutions<sup>62</sup>. When applied to the array of fluxes we find that this requirement leads to the same boundary conditions as in 61. In terms of  $(u, v)$  these boundary conditions in the vicinity of fluxes are

$$\sqrt{r} \begin{pmatrix} u \\ v \end{pmatrix} \rightarrow \cos \theta e^{-i\phi} \begin{pmatrix} 1 \\ i \end{pmatrix} + \sin \theta \begin{pmatrix} i \\ 1 \end{pmatrix} \quad \text{for } +\frac{\Phi_0}{2} \text{ fluxes} \quad (20)$$

$$\sqrt{r} \begin{pmatrix} u \\ v \end{pmatrix} \rightarrow \cos \theta \begin{pmatrix} 1 \\ i \end{pmatrix} + \sin \theta e^{i\phi} \begin{pmatrix} i \\ 1 \end{pmatrix} \quad \text{for } -\frac{\Phi_0}{2} \text{ fluxes.} \quad (21)$$



These boundary conditions are actually equivalent to those of Ref. 61.

For the present problem of  $d$ -wave quasiparticles in a vortex lattice the above requirement of self-adjointness  $D(H) = D(H^*)$  translates into the following boundary conditions near A vortices:

$$\sqrt{r}\psi(\mathbf{R}_A + \mathbf{r}) \rightarrow \cos\theta e^{\frac{i\cos\varphi}{2}} \begin{pmatrix} e^{-i\varphi} - i \\ ie^{-i\varphi} - 1 \end{pmatrix} + \sin\theta e^{-\frac{i\cos\varphi}{2}} \begin{pmatrix} e^{-i\varphi} + i \\ ie^{-i\varphi} + 1 \end{pmatrix}. \quad (22)$$

The boundary conditions at B vortices differ by the overall phase factor  $\exp(i\varphi)$ :

$$\sqrt{r}\psi(\mathbf{R}_B + \mathbf{r}) \rightarrow \cos\theta e^{\frac{i\cos\varphi}{2}} \begin{pmatrix} 1 - ie^{i\varphi} \\ i - e^{i\varphi} \end{pmatrix} + \sin\theta e^{-\frac{i\cos\varphi}{2}} \begin{pmatrix} 1 + ie^{i\varphi} \\ i + e^{i\varphi} \end{pmatrix}. \quad (23)$$

Thus, if the interior of a vortex is treated as a black box, in order to fully specify the problem, the linearized Hamiltonian  $H_{FT}$  must be supplemented by boundary conditions at the locations of vortices<sup>10</sup>. Every boundary condition depends on a single parameter  $\theta$ , which is easily shown to be independent of an A-B assignment. Indeed, the transformation from one choice of A and B sublattices to another is given by a unitary matrix

$$U_{AA'} = \begin{pmatrix} e^{i\phi_A - i\phi_{A'}} & 0 \\ 0 & e^{i\phi_B' - i\phi_B} \end{pmatrix} = e^{i\phi_A - i\phi_{A'}} \cdot \mathbf{1},$$

since  $\phi_A + \phi_B = \phi_{A'} + \phi_{B'} = \phi(\mathbf{r})$ .  $U_{AA'}$  is proportional to unit matrix, and the asymptotic behavior of the wavefunctions, specified by  $\theta$ , is clearly invariant under all such transformations. Note that parameter  $\theta$  for a given vortex has been intentionally defined in this particular way for convenience. It is independent on whether this individual vortex belongs to an A or a B sublattice, and is therefore a scalar under FT singular gauge transformations. Naturally, one must recall here that the actual form of the boundary condition *does* change according to Eqs. (22,23) depending on whether a particular vortex belongs to an A or a B sublattice. Furthermore, note that there is no *a priori* requirement that parameters  $\theta$  are equal for different vortices within unit cell. Just as in the case of a single Dirac string, parameters  $\theta$  cannot be determined from the linearized Hamiltonian. Rather, the boundary conditions  $\theta$  are determined by the short-ranged physics of fully self-consistent BdG equations and include all effects of higher orders in  $(k_{Fl})^{-1}$  expansion.

Equipped with this new understanding we now revisit the “ABAB vs. AABB” problem and consider the numerical computations performed earlier<sup>8,10</sup>. There boundary conditions were not explicitly enforced and the numerical procedure itself “spontaneously” selected a particular set of boundary conditions. In calculations done in 8,10, the wavefunctions are represented as linear combinations of

plane waves, and, after a substitution into the linearized FT Hamiltonian, the series is truncated at some number of terms  $N = (2n+1)^2$ , which is gradually increased until convergence is achieved:

$$\psi_{\mathbf{k},n}(\mathbf{r}) = e^{i\mathbf{k}\mathbf{r}} \sum_{\mathbf{G} \in \Sigma_N} e^{i\mathbf{G}\cdot\mathbf{r}} \begin{pmatrix} u_{\mathbf{G}} \\ v_{\mathbf{G}} \end{pmatrix}. \quad (24)$$

Rather than analyzing the spectra we first concentrate on the wavefunctions. The solutions  $\psi(\mathbf{r}) = (u(\mathbf{r}), v(\mathbf{r}))$  are shown in Fig. 3. The wavefunctions indeed approach  $1/\sqrt{r}$  dependence on the distance from the vortex as the number of reciprocal lattice vectors included in the solution is increased. The values of  $\theta$  for  $\psi_n(\mathbf{k})$  can be extracted from the wavefunctions by various methods. As an example, the procedure involving ratios  $\lim_{\rho \rightarrow 0} |u(\rho, \varphi = 0)|/|v(\rho, \varphi = 0)|$  is illustrated in Fig. 3. Since there are two vortices per unit cell<sup>8</sup> we label them “A” and “B” to indicate their belonging to two different sublattices – to avoid any confusion, it is important to stress here that the labels “A” and “B” refer to *two physically distinct* vortices rather than to an FT gauge label attached to an individual vortex (the quotation marks are used to highlight this difference). The value  $\theta$  for vortex “A” turns out to be close to  $\theta = (0.75 \pm 0.03)\pi$ , while vortex “B” has asymptotic form with  $\theta = (0.25 \pm 0.03)\pi$ . The conclusion remains valid not only for the vicinity of nodal points, but also for all bands at arbitrary  $\mathbf{k}$  for which  $\theta$ 's could be extracted. As discussed in a separate paper,<sup>47</sup> these values of  $\theta$ 's are among several consistent with the general symmetry requirements that must be obeyed by the solutions of the full BdG equations. They thus faithfully represent a possible solution for the low energy spectrum of BdG equations. The meaningful determination of  $\theta$  for high energy bands was beyond the precision of our calculations since the contribution of the singular part of the wavefunctions decreases for higher bands, and one has to consider distances that are extremely close to the vortex to extract the asymptotic  $1/\sqrt{r}$  behavior. This, in turn requires diagonalization of matrices with unrealistically large  $N$ .

We then performed a similar analysis of several other arrangements of A and B sublattices. We found that the eigenstates of “AABB” and “ABAB” lattices for four vortices per unit cell and similar vortex lattices rotated by  $\pi/4$  with respect to the nodal directions also exhibit the same pattern: the plane wave expansion procedure drives “A” vortices to  $\theta \approx 0.75\pi$  and “B” vortices to  $\theta \approx 0.25\pi$ . The discrepancies encountered earlier that gave rise to the “ABAB vs. AABB” problem<sup>10</sup> are now easy to understand, since the problems solved without externally imposing boundary conditions at vortex sites corresponded to physically *different* situations once boundary conditions were “spontaneously” generated by the chosen procedure, i.e. the two problems solved were *not connected* by an FT singular gauge transformation. In particular, the “ABAB” sublattice partition corresponds to the boundary conditions at vortex locations with  $\theta = \pm\pi/4$  assigned in a checkerboard arrangement.

In contrast, if vortices ‘‘A’’ and ‘‘B’’ are chosen to form series of parallel lines, as in the ‘‘AABB’’ partitioning, the numerical procedure spontaneously selects boundary conditions arranged as interchanging lines of  $\theta = \pi/4$  and  $\theta = -\pi/4$ . Obviously, these are two genuinely different physical situations in light of the condition that  $\theta$  for a particular vortex must remain unchanged under FT gauge transformations.

It is clear that the boundary conditions at vortex locations must be fixed separately and changed appropriately under FT transformation following Eqs. (22,23), as anticipated in 10. A specific  $\theta$  assignment can be implemented by a procedure which represents a modification of a plane wave expansion similar to the orthogonalized plane waves method. This procedure is introduced and discussed in detail in section V and yields results in mutual agreement for different FT singular gauge choices. Alternatively, the boundary conditions can be emulated by adding a mass term to the linearized Hamiltonian that grows rapidly as one approaches a vortex core. The latter approach is described in section VI.

Group element $h$	Transformation of $\mathbf{v}$ and $\mathbf{a}$
Mirror symmetry $m_x$ : $m_x \mathbf{r} = (l/2 - x, y)$	$v_x(g\mathbf{r}) = v_x(\mathbf{r})$ $v_y(g\mathbf{r}) = -v_y(\mathbf{r})$ $a_x(g\mathbf{r}) = a_x(\mathbf{r})$ $a_y(g\mathbf{r}) = -a_y(\mathbf{r})$
Mirror symmetry $m_y$ : $m_y \mathbf{r} = (x, l/2 - y)$	$v_x(g\mathbf{r}) = -v_x(\mathbf{r})$ $v_y(g\mathbf{r}) = v_y(\mathbf{r})$ $a_x(g\mathbf{r}) = -a_x(\mathbf{r})$ $a_y(g\mathbf{r}) = a_y(\mathbf{r})$
Inversion $I = m_x m_y$ : $I\mathbf{r} = 2\mathbf{R}_A - \mathbf{r}$	$\mathbf{v}(g\mathbf{r}) = -\mathbf{v}(\mathbf{r})$ $\mathbf{a}(g\mathbf{r}) = -\mathbf{a}(\mathbf{r})$
Inversion $A \rightarrow B$ : $P\mathbf{r} = -\mathbf{r}$	$\mathbf{v}(g\mathbf{r}) = -\mathbf{v}(\mathbf{r})$ $\mathbf{a}(g\mathbf{r}) = \mathbf{a}(\mathbf{r})$
$Pm_x \mathbf{r} = (x + l/2, -y)$	$v_x(g\mathbf{r}) = -v_x(\mathbf{r})$ $v_y(g\mathbf{r}) = v_y(\mathbf{r})$ $a_x(g\mathbf{r}) = a_x(\mathbf{r})$ $a_y(g\mathbf{r}) = -a_y(\mathbf{r})$
$Pm_y \mathbf{r} = (-x, y + l/2)$	$v_x(g\mathbf{r}) = v_x(\mathbf{r})$ $v_y(g\mathbf{r}) = -v_y(\mathbf{r})$ $a_x(g\mathbf{r}) = -a_x(\mathbf{r})$ $a_y(g\mathbf{r}) = a_y(\mathbf{r})$
Translation $s = PI$ : $s\mathbf{r} = \mathbf{r} + 2\mathbf{R}_A$	$\mathbf{v}(g\mathbf{r}) = \mathbf{v}(\mathbf{r})$ $\mathbf{a}(g\mathbf{r}) = -\mathbf{a}(\mathbf{r})$

TABLE I: Symmetry properties of superfluid velocity  $\mathbf{v}$  and internal gauge field  $\mathbf{a}$ .

#### IV. SYMMETRIES OF THE SINGLE-NODE HAMILTONIAN

In the previous section we showed that the linearized FT Hamiltonian  $H_{FT}$  must be supplemented by boundary conditions at vortex locations. These boundary conditions are fixed by a dimensionless parameter  $\theta \in [0, \pi)$ . The specific value of  $\theta$  that should be used is determined by the physics unfolding at the lengthscales shorter than those included in the linearized description. Thus, we are at an impasse; we apparently must solve for the physics beyond linearization to fully specify the linearized problem itself. We take the initial step toward such a solu-

tion in a separate paper,<sup>47</sup> where we study a lattice  $d$ -wave superconductor. In the present paper, we continue our analysis of different  $\theta$ 's by focusing on the symmetry properties of  $H_{FT}$  in combination with those of the original, non-linearized BdG problem (2,5).

Certain aspects of the symmetry properties of the linearized Hamiltonian  $H_{FT}$  were already considered previously<sup>9,12</sup>. For example, it has been shown that the Dirac node of the zero-field problem is not destroyed by the inversion-symmetric vortex lattice; the only situation considered, however, is the one with no boundary conditions imposed on the vortices. Here, we extend and generalize these early results by analyzing the complete group of symmetry transformations of  $H_{FT}$  and examine the consequences of imposing the boundary conditions (22,23). For convenience, only the simplest choice of a unit cell (Fig. 1) containing two vortices per unit cell will be studied. Using the Fourier representation (A4) and (A5), the superfluid velocity  $\mathbf{v}(\mathbf{r})$  and the internal gauge field  $\mathbf{a}(\mathbf{r})$  can be shown to transform under geometric point transformations  $h$  according to Table I. Note that under inversion  $I$  around a vortex both  $\mathbf{v}(\mathbf{r})$  and  $\mathbf{a}(\mathbf{r})$  change sign, while the inversion operation  $P$  around the midpoint between vortex A and vortex B which interchanges vortices A and B, leaves the internal gauge field  $\mathbf{a}(\mathbf{r})$  invariant:  $\mathbf{a}(-\mathbf{r}) = \mathbf{a}(\mathbf{r})$ .

The operations  $h$  do not form a group by themselves, since their product can generate a pure translation by a lattice vector. Rather, the group is formed by elements  $T_{\mathbf{R}}h$  where  $T_{\mathbf{R}}$  is an arbitrary translation by a lattice vector  $\mathbf{R}$ . One can easily check that the group can be generated by forming products of primitive translations, reflections  $m_x$ ,  $m_y$  and an inversion  $P$ . The symmetry of the potentials  $\mathbf{v}(\mathbf{r})$  and  $\mathbf{a}(\mathbf{r})$  is higher than the group just described, including also operations generated by rotations by  $\pi/4$  around a vortex; these additional operations, however, do not correspond to any symmetry of the linearized Hamiltonian due to the last term in (9) reflecting the fact that the boost in the direction of one of the nodes breaks the four-fold symmetry of the original BdG Hamiltonian even in the isotropic case  $v_F = v_{\Delta}$ . Only after the contributions of all four nodes are combined, will this symmetry be fully restored.

It should be emphasized that the symmetry properties discussed in this section refer to the linearized Hamiltonian  $H_{FT}$  and its eigenfunctions  $\psi(\mathbf{r})$ .  $\psi(\mathbf{r})$  are related to the wavefunctions  $\Psi(\mathbf{r})$  in the original BdG basis according to

$$\Psi(\mathbf{r}) = e^{ik_F x} \begin{pmatrix} e^{i\phi_A(\mathbf{r})} & 0 \\ 0 & e^{-i\phi_B(\mathbf{r})} \end{pmatrix} \psi(\mathbf{r}).$$

All transformations introduced above are understood as *intra-nodal*. For example, inversion  $P$  transforms  $\psi(\mathbf{r})$  to  $\psi(-\mathbf{r})$ , and the transformed wavefunction in the original basis is given by

$$P\Psi(\mathbf{r}) = e^{ik_F x} \begin{pmatrix} e^{i\phi_A(\mathbf{r})} & 0 \\ 0 & e^{-i\phi_B(\mathbf{r})} \end{pmatrix} \psi(-\mathbf{r}) . \quad (25)$$

Properties of the original non-linearized Hamiltonian (5) under various symmetry operations and their relation to the symmetries of  $\mathcal{H}_{FT}$  will be discussed separately in section VI.

Before analyzing the problem with imposed boundary conditions, we first consider formally the linearized Hamiltonian  $\mathcal{H}_{FT}$  with no boundary conditions enforced at vortex locations. Although such “unrestricted” problem is in principle not guaranteed to represent any particular physically meaningful linearization of the full BdG Hamiltonian (2), this discussion will serve as the basis for subsequent analysis. After the boundary conditions are enforced, the allowed symmetry operations will form a subset of the full transformation group of the “unrestricted” Hamiltonian, which depends on the choice of the self-adjoint extension.

Using the properties of superfluid velocities from Table I it is straightforward to verify that if  $\Psi_{\mathbf{k}}$  is an eigenfunction of Hamiltonian  $\mathcal{H}_{FT}$  with crystal momentum  $\mathbf{k}$  and eigenvalue  $E$  then  $\Psi'_{\mathbf{k}'} = D(g)\Psi_{\mathbf{k}}$  is an eigenfunction of  $\mathcal{H}_{FT}$  with crystal momentum and eigenvalue  $\pm E$  according to the Table III in the Appendix. In identifying  $\mathbf{k}'$  after the transformations involving phase factor

$$f(\mathbf{r}) \equiv \exp(-i\delta\phi) \equiv \exp(i\phi_B - i\phi_A)$$

it is important to keep in mind that  $f(\mathbf{r})$  is not periodic but anti-periodic – it changes sign under primitive translations along  $x$  and  $y$  directions (see Appendix):

$$f(x+l, y) = -f(x, y) \quad (26)$$

$$f(x, y+l) = -f(x, y) \quad (27)$$

Transformations  $D(g)$  form ray representation<sup>67</sup> of the group, and the standard methods can be applied to analyze the degeneracy of the eigenstates. In addition to geometric transformations and pure translations  $D(T_{\mathbf{R}})$ , there is an additional anti-linear complex-conjugation transformation:

$$D(C)\Psi = ie^{-i\delta\phi}\sigma_2\bar{\Psi}$$

$D(C)$  commutes with all other operators up to a phase factor, and combined with the operations listed in the left portion of Table III from Appendix,  $C$  generates 8 new eigenfunctions with energy  $\pm E$ . Since Bloch basis has already been chosen to diagonalize ordinary translation operators we have the total of 16 non-trivial transformations, which generate 8 eigenfunctions with energy  $E$  and 8 eigenfunctions with energy  $-E$ .

If  $\mathbf{k}$  is an arbitrary point of the Brillouin zone that does not lie on one of the symmetry lines, all 8 states with energy  $E$  correspond to distinct crystal momenta  $\mathbf{k}'$  forming a “star” shown in Fig. 4, and are therefore linearly independent. Consequently, for general  $\mathbf{k}$  the symmetry of the Hamiltonian is not sufficient to result in degeneracy of the bands at the same  $\mathbf{k}$ . For every state  $(E, \mathbf{k})$  there is a state with the opposite energy  $(-E, \mathbf{k})$  obtained by applying transformation  $CP$  to the original wavefunction and seven other pairs of states with

energies  $\pm E$  with crystal momenta  $\mathbf{k}'$  belonging to the “star”. For certain particularly symmetric values of  $\mathbf{k}$  two or more points of the “star” coincide, and therefore the spectrum may become degenerate, as will be discussed shortly in detail after the boundary conditions are chosen. Note, however, that the Hamiltonian apparently possesses higher symmetry than what is reflected in the band structure spectrum shown in Fig. 5, which was obtained numerically by the plane wave expansion (without imposing boundary conditions explicitly near vortices)<sup>8,9,10</sup>. In particular, the symmetry analysis indicates that the node at  $\mathbf{k} = 0$  implies also the identical node centered around the corner of the Brillouin zone  $\pi$ , while no such additional nodes are seen in numerical computation. In view of our previous discussion of the role of boundary conditions, the discrepancy is easy to understand: we have shown that, even if the boundary conditions at the vortices are not explicitly enforced from the outset, the numerical procedure selects a certain self-adjoint extension, which has the effect of reducing the symmetry of the problem.

To study the effect of boundary conditions on the symmetry of the spectrum, we note that, if one starts with Hamiltonian  $\mathcal{H}_{FT}$  with boundary conditions on the wavefunctions  $\psi(\mathbf{r})$  given by parameters  $\theta_{1(2)}$  near the two vortices, then after general transformation wavefunctions  $D(g)\psi(\mathbf{r})$  have asymptotics described by a set of different boundary conditions  $\theta'_{1(2)}$ . The new parameters  $\theta'_{1(2)}$  are shown in the rightmost column of Table III from Appendix. Note that the spectrum is symmetric under  $(\mathbf{k}, E) \rightarrow (\mathbf{k}, -E)$  and only if  $\theta_1 = -\theta_2$ . In the case when  $\theta_1 = \theta_2$  that leads to only two possible choices:  $\theta_1 = \theta_2 = 0$  and  $\theta_1 = \theta_2 = \pi/2$ . For these extensions, however, the inversion property  $E(\mathbf{k}) = E(-\mathbf{k})$  is lost and we find that no self-adjoint extension exists with the spectrum resembling that of the zero-field Dirac particles, if all vortices are assigned the same value of  $\theta$ .

*Plane wave extension.* The numerical analysis of section III showed that the straightforward plane wave expansion “spontaneously” generates solutions with the boundary conditions  $\theta_{1(2)} \approx \pm\pi/4$ . We now first demonstrate that the spectrum of the self-adjoint extension with  $\theta_{1(2)} = \pm\pi/4$  indeed has the symmetry properties consistent with the numerical solution and then clarify why the plane wave expansion procedure favors these particular boundary conditions.

The subset of symmetry operations that leaves  $\theta_{1(2)} = \pi/4$  invariant and its star of the  $\mathbf{k}$ -vectors is shown in Fig. 5. The special points in BZ where the spectrum can potentially become degenerate are  $\Gamma$ ,  $X$ ,  $Y$ , and  $M$ , where all four vectors of the star coincide<sup>68</sup>. Whether this indeed leads to degenerate eigenfunctions depends on  $\mathbf{k}$  and should be analyzed in each case separately. Using Table III from Appendix, the representation matrices  $D(PM_y) = g_1$ ,  $D(CPI) = g_2$ , and  $D(Cm_x) = g_3$  satisfy

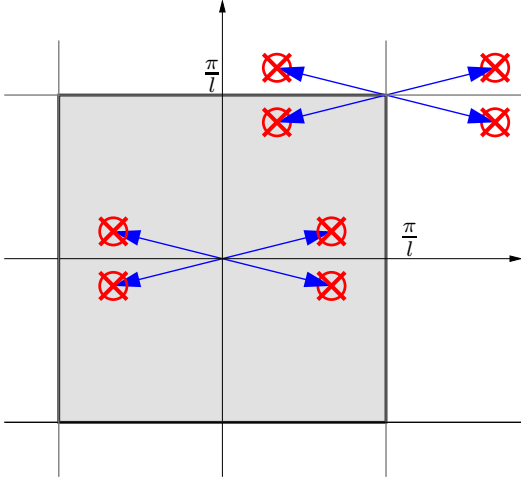


FIG. 4: First Brillouin zone is shown with the star of wavefunctions generated by applying symmetry operations to  $\Psi_{\mathbf{k}}(\mathbf{r})$ . For convenience both, positive energy states (open circles) and negative energy eigenfunctions (crosses) are shown.

$$\begin{aligned}
 g_1^2 &= e^{ik_y l} & g_1 g_2 &= i e^{-ik_y l} g_3 & g_1 g_3 &= -i g_2 \\
 g_2 \overline{g_1} &= -i e^{i(k_x - k_y)l} g_3 & g_2 \overline{g_2} &= -e^{i(k_x + k_y)l} & g_2 \overline{g_3} &= i g_1 \\
 g_3 \overline{g_1} &= i e^{ik_x l} g_2 & g_3 \overline{g_2} &= i e^{ik_x l} g_1 & g_3 \overline{g_3} &= 1
 \end{aligned} \tag{28}$$

At  $\Gamma$  and  $M$ -points  $g_2 \overline{g_2} = -1$  and consequently there are no one-dimensional representations. The lowest dimension of irreducible representation of relations (28), realized by Pauli matrices  $g_i = \sigma_i$ , is two. Thus, the eigenstates in the center and in the corner of the BZ are at least doubly degenerate.

At points  $X$  and  $Y$  of Brillouin zone

$$g_2^2 \Psi(\mathbf{r}) = \Psi(\mathbf{r}),$$

and there are two one-dimensional representations  $g_1 = \pm 1$ ,  $g_2 = \pm i\lambda$ , and  $g_3 = \lambda$ , where  $\lambda$  is an arbitrary complex parameter with unit norm  $|\lambda| = 1$ . The energy bands therefore are non-degenerate at  $X$  and  $Y$ . These results are in complete agreement with the numerical solution obtained by Franz and Tešanović<sup>8</sup> which is shown in Fig. 5.

To understand why the boundary conditions with  $\theta_{1(2)} = \pm\pi/4$  are favored by the plane wave expansion procedure, we recall that in this method the eigenfunctions of  $\mathcal{H}_{FT}$  are sought as

$$\psi_{\mathbf{k}}(\mathbf{r}) = \sum_{\mathbf{Q} \in \Sigma_N} \begin{pmatrix} u_{\mathbf{Q}}^{\mathbf{k}} \\ v_{\mathbf{Q}}^{\mathbf{k}} \end{pmatrix} e^{i(\mathbf{Q}+\mathbf{k})\mathbf{r}} \tag{29}$$

where the set of reciprocal lattice vectors  $\Sigma_N$  in the expansion form a square grid  $(2N+1) \times (2N+1)$ :

$$\Sigma_N = \left\{ \frac{2\pi}{l}(m, n) : -N \leq m, n \leq N \right\}, \tag{30}$$

where  $m$  and  $n$  are integers. Here we make an assumption, well justified by numerical calculations, that the procedure produces convergent result as the number of plane waves in the expansion (29) is increased. Note that the choice of subset  $\Sigma_N$  of reciprocal lattice vectors  $\mathbf{Q}$  is crucial, since the matrix elements decrease only as  $1/|\mathbf{Q}|$  for large momenta, and if the matrix in reciprocal space was truncated differently, the eigenstates could end up corresponding to a *different* self-adjoint extension. After substitution into Hamiltonian  $\mathcal{H}_{FT}$  the coefficients  $\Psi_{\mathbf{Q}}^{\mathbf{k}} = (u_{\mathbf{Q}}^{\mathbf{k}}, v_{\mathbf{Q}}^{\mathbf{k}})$  can be found by diagonalization of the Fourier-transformed equations

$$H_0(\mathbf{k} + \mathbf{Q})\Psi_{\mathbf{Q}}^{\mathbf{k}} + \sum_{\mathbf{Q}' \in \Sigma_N} \hat{V}(\mathbf{Q} - \mathbf{Q}') \Psi_{\mathbf{Q}'}^{\mathbf{k}} = E\Psi_{\mathbf{Q}}^{\mathbf{k}}, \tag{31}$$

where the summation is performed over all reciprocal vectors  $\mathbf{Q}' \in \Sigma_N$  except  $\mathbf{Q}' = \mathbf{Q}$ , the zero field Hamiltonian  $H_0(\mathbf{p})$  is

$$H_0(\mathbf{p}) = \sigma_3 p_x + \sigma_1 p_y,$$

and  $(i\pi\hbar v_{BZ})^{-1}Q^2 \hat{V}(\mathbf{Q})$  is given by

$$\begin{pmatrix} Q_y e^{-i\mathbf{Q}\cdot\mathbf{R}_A} & \frac{Q_x}{2} (e^{-i\mathbf{Q}\cdot\mathbf{R}_B} - e^{-i\mathbf{Q}\cdot\mathbf{R}_A}) \\ \frac{Q_x}{2} (e^{-i\mathbf{Q}\cdot\mathbf{R}_B} - e^{-i\mathbf{Q}\cdot\mathbf{R}_A}) & Q_y e^{-i\mathbf{Q}\cdot\mathbf{R}_B} \end{pmatrix}$$

Using identities  $\hat{V}(-\mathbf{Q}) = \overline{\hat{V}(\mathbf{Q})} = -\sigma_2 V(\mathbf{Q}) \sigma_2$  and  $\sigma_2 H_0 \sigma_2 = -H_0$  it is easy to verify that if  $\Psi_{\mathbf{Q}}^{\mathbf{k}}$  is the eigenfunction of (31) with momentum  $\mathbf{k}$  and energy  $E$  then

$$\Psi'_{\mathbf{Q}} = \sigma_2 \overline{\Psi_{\mathbf{Q}}^{\mathbf{k}}}, \quad \mathbf{Q} \in \Sigma_N$$

is also a solution of (31) with momentum  $\mathbf{k}$  and energy  $-E$ . In real space the new wavefunction corresponds to  $\Psi'(\mathbf{r}) = CP\Psi(\mathbf{r}) = \sigma_2 \Psi(-\mathbf{r})$ . Similarly, from identity  $\hat{V}(\mathbf{Q}) = -e^{2\mathbf{Q}\cdot\mathbf{R}_A} \hat{V}(-\mathbf{Q})$  we can obtain another eigenstate

$$\Psi''_{\mathbf{Q}} = \Psi_{-\mathbf{Q}}^{\mathbf{k}} e^{2\mathbf{Q}\cdot\mathbf{R}_A}, \quad \mathbf{Q} \in \Sigma_N$$

with with energy  $-E$  but inverted Bloch momentum  $-\mathbf{k}$ . In real space the new wavefunction is described by  $I\Psi = \Psi(2\mathbf{R}_A - \mathbf{r})$ . In fact using the properties of matrix elements  $\hat{V}$  it is straightforward to show that all transformations of Table III from Appendix that do not involve factors  $e^{-i\delta\phi}$  are exact symmetries of the Hamiltonian (31) for any finite  $N$ . According to our assumption the procedure converges to a solution, which corresponds to some self-adjoint extension described by certain  $\theta_{1(2)}$ . By inspection, we find from Table III from Appendix that the only choice of  $\theta_{1(2)}$  ensuring the above symmetries are satisfied for arbitrary finite  $N$  is  $\theta_{1(2)} = \pm\pi/4$ .

We conclude by demonstrating that this self-adjoint extension has a single nodal point with zero energy at  $\mathbf{k} = 0$ . Since Hamiltonian  $\mathcal{H}_{FT}$  does not possess a small parameter, and both the scalar and vector potentials  $\mathbf{v}$

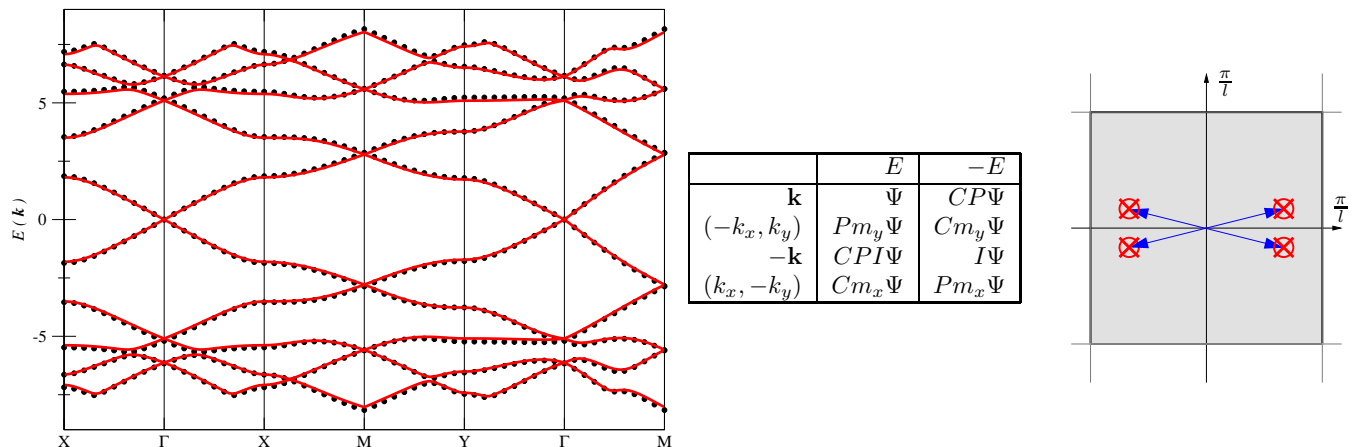


FIG. 5: Left panel: the energy bands of linearized Hamiltonian for two vortices per unit cell calculated by plane wave expansion<sup>8</sup> (solid lines) and by OPW method with boundary conditions  $\theta_A = -\pi/4$  and  $\theta_B = +\pi/4$  (dots). Center panel: symmetry operations relating eigenenergies at different  $\mathbf{k}$ . Right panel: the first Brillouin zone with equivalent  $\mathbf{k}$  vectors shown by circles. For every state with energy  $E$  at momentum  $\mathbf{k}$  there is a state with the same momentum and energy  $-E$ .

and  $\mathbf{a}$  are singular near vortices, it is desirable to base the discussion on non-perturbative argument. Such an argument was suggested by Vishwanath<sup>11,12</sup>, who made use of two properties of the energy spectrum at  $\mathbf{k} = 0$ . First, all states are doubly degenerate at  $\mathbf{k} = 0$ , second, for each state  $(\mathbf{k}, E)$  there is another state  $(\mathbf{k}, -E)$ . He noted that the two properties are shared by the zero-field problem, which has a pair of states at zero energy and symmetrically located pairs of states at  $E_n$  and  $E_{-n}$ , where  $n$  is the band index. Thus, the number of states is  $2(2n_{max} + 1)$ , where  $n_{max}$  is a heuristic parameter denoting the number of bands with positive energy after fictitious ultraviolet cut-off is introduced in order to make the spectrum bounded. According to Vishwanath, since the total number of states is preserved after the potentials  $\mathbf{v}$  and  $\mathbf{a}$  are turned on, the pairs of degenerate states of  $\mathcal{H}_{FT}$  must also be centered around zero. Otherwise the total number states in the system would have been a  $2(2n_{max})$ .

The argument in the form just presented might seem ill-defined and lead to inconsistent results. Indeed, if applied blindly, it would falsely suggest that the spectrum should also be gapless at the corner of the Brillouin zone. Certainly, the number of states at the center and the corner of BZ must be the same for any reasonable high-energy cut-off and therefore should be equal to  $2(2n_{max} + 1)$ . Just as for the states at the center of BZ, the states at the corner are doubly degenerate, and for each pair of states there is a symmetric pair with the opposite energy. Thus, one might conclude, there must be a pair of states precisely at zero energy not only for the  $\mathcal{H}_{FT}$  but also for the zero-field problem! Yet, the spectrum at the corner of BZ is gapped.

Clearly, the difficulties one encounters by applying the above argument literally are related to the high-energy cut-off and have a technical character. We show below

that Vishwanath's construction<sup>69</sup> can be made precise in the framework of the self-adjoint extensions adopted in this article. We have seen that the plane wave expansion corresponds to the extension characterized by  $\theta_{1(2)} = \pm\pi/4$  if the set of reciprocal wave vectors of the basis forms a square grid (30) as  $N \rightarrow \infty$ . At each finite  $N$ , there are  $(2N + 1)^2$  reciprocal lattice vectors  $\mathbf{Q}$  contained in the grid  $\Sigma_N$  and each  $\mathbf{Q}$  is associated with two basis vectors  $(1, 0)$  and  $(0, 1)$ . Thus the dimensionality of the basis is  $2(2N + 1)^2$ . Since even for finite  $N$  the solutions at  $\mathbf{k} = 0$  appear as doublets at energy  $E$  and another doublet at  $-E$ , the argument of Vishwanath can be directly applied, and one of the doublets should occupy  $E = 0$ , otherwise the number of states would have been a multiple of 4 rather than  $2(2N + 1)^2$ .

It is interesting to observe why the same argument cannot be applied to the eigenfunctions of  $\mathcal{H}_{FT}$  at the corner of the Brillouin zone, and the spectrum remains gapped. Although at  $\mathbf{k} = \pi$  the spectrum is degenerate in the limit of infinite grid of reciprocal lattice vectors, for finite  $N$  the degeneracy is only approximate. As  $N$  is increased, the low energy bands become nearly degenerate, however at high enough energies the spectrum at  $\mathbf{k} = \pi$  remains corrupted. Transformation  $g_2 = D(CPI)$ , which ensured the degeneracy of the spectrum at  $\mathbf{k} = 0$  due to  $g_2\bar{g}_2 = -1$  even for finite  $N$  does not have the same effect on the states at  $\mathbf{k} = \pi$ . Certainly, after applying  $g_2$  to an eigenstate  $\psi_\pi$  with momentum  $\pi$  and energy  $E$ , one still obtains an eigenstate  $\psi_{-\pi} = g_2\psi_\pi$  with the same energy, but with momentum  $-\pi$ . The situation is shown schematically in Fig. 6. Although for infinite  $N$  the points  $\pi$  and  $-\pi$  are equivalent, for any finite  $N$  the wavefunctions describing the two states contain different set of reciprocal lattice vectors, and therefore are distinct. In the analysis of the degeneracy of the states the two values of  $\mathbf{k}$  should be considered as independent.

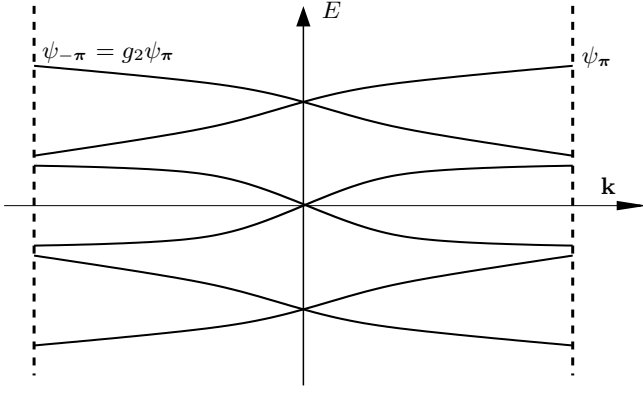


FIG. 6: Schematic representation of the spectrum at finite  $N$ . The small gaps between given two neighboring bands at the corner of Brillouin zone decrease to zero in the limit of infinite  $N$ .

Thus the argument on zero-modes cannot be applied at the corner of Brillouin zone and for  $\theta_{1(2)} = \pm\pi/4$  there is a single Dirac node at  $\Gamma$ -point  $\mathbf{k} = 0$ .

## V. NUMERICAL ANALYSIS

As we have shown, the straightforward expansion of wavefunctions  $\psi_{\mathbf{k}}(\mathbf{r})$  in the plane wave basis

$$e^{i\mathbf{q}\cdot\mathbf{r}} \begin{pmatrix} 1 \\ 0 \end{pmatrix} \quad \text{and} \quad e^{i\mathbf{q}\cdot\mathbf{r}} \begin{pmatrix} 0 \\ 1 \end{pmatrix}$$

where  $\mathbf{q} = \mathbf{k} + \mathbf{Q}$ ,  $\mathbf{Q} \in \Sigma$  is problematic since the matrix elements of the Hamiltonian decrease only as  $1/|\mathbf{Q}|$  because of the singular nature of the perturbation potentials at vortex locations. Consequently the eigenvalues of the linearized Hamiltonian depend on the way the matrix  $\langle \mathbf{q}' | H | \mathbf{q} \rangle$  is truncated and consistent ultraviolet cut-offs are parameterized by parameters  $\theta$  specifying the boundary conditions at each vortex. For example, the symmetric choice of the set  $\mathbf{Q} \in \Sigma_N$  results in a choice  $\theta_{1(2)} = \pm\pi/4$ . To enforce the desired boundary conditions we use a procedure similar to orthogonalized plane waves method used in the standard band theory. Instead of expanding the wavefunctions  $\psi(r)$  in plane wave basis we define

$$\tilde{\chi}(\mathbf{R}_i + \mathbf{r}) = \frac{e^{-r^2/a^2}}{(2\pi)^{3/4}\sqrt{ar}} \left( \sin\theta e^{\frac{i}{2}\cos\phi} \begin{pmatrix} e^{-i\phi} - i \\ ie^{-i\phi} - 1 \end{pmatrix} - \cos\theta e^{-\frac{i}{2}\cos\phi} \begin{pmatrix} e^{i\phi} + i \\ ie^{-i\phi} + 1 \end{pmatrix} \right) \quad (32)$$

if  $\mathbf{R}_i$  is an  $A$  vortex, and

$$\tilde{\chi}(\mathbf{R}_i + \mathbf{r}) = \frac{e^{-r^2/a^2}}{(2\pi)^{3/4}\sqrt{ar}} \left( \sin\theta e^{\frac{i}{2}\cos\phi} \begin{pmatrix} 1 - ie^{i\phi} \\ i - e^{i\phi} \end{pmatrix} - \cos\theta e^{-\frac{i}{2}\cos\phi} \begin{pmatrix} 1 + ie^{i\phi} \\ i + e^{-i\phi} \end{pmatrix} \right). \quad (33)$$

if  $\mathbf{R}_i$  belongs to class  $B$ . The wavefunctions that have the same asymptotics at the vortices and Bloch periodicity can easily then be constructed as

$$\chi_{\mathbf{q}}(\mathbf{r}) = \sum_{\mathbf{R}} e^{i\mathbf{q}\cdot\mathbf{R}} \chi(\mathbf{r} + \mathbf{R})$$

The wavefunctions are orthogonal to the singular parts of asymptotics (10). The appropriate basis for expansion of the eigenfunctions of the Hamiltonian  $\mathcal{H}_{FT}$  with boundary conditions  $\{\theta_i\}$  is

$$e^{i\mathbf{q}\cdot\mathbf{r}} \begin{pmatrix} 1 \\ 0 \end{pmatrix} - \sum_i \alpha_{\mathbf{q}}^i \chi^i(\mathbf{r}) \quad \text{and} \quad e^{i\mathbf{q}\cdot\mathbf{r}} \begin{pmatrix} 0 \\ 1 \end{pmatrix} - \sum_i \beta_{\mathbf{q}}^i \chi^i(\mathbf{r})$$

where cutoff  $a$  is introduced for numerical convenience. The coefficients  $\alpha_{\mathbf{q}}^i$  and  $\beta_{\mathbf{q}}^i$  are chosen so that the basis functions are orthogonal to  $\chi^i(\mathbf{r})$ . In the limit  $a \rightarrow 0$  the procedure ensures that the modes with asymptotics orthogonal to those given by  $\theta$  are projected out. Because of the exponential factors introduced in  $\chi(\mathbf{r})$  the largest reciprocal vector  $\mathbf{Q}$  should be of order  $1/a$  or larger, so that there is appreciable region around a vortex  $1/Q_{max} < r < a$  where the wavefunctions have the desired  $1/\sqrt{r}$  asymptotics but still are not affected by the exponential factors. We typically used  $a = 0.05l$  and increased the number of basis elements until the convergence is achieved. Further decrease of the damping parameter  $a$  affects the results very weakly. Examples of the energy bands obtained by this method for two vortices per unit cell for different boundary conditions are shown in Figs. 5 and 7. The first figure shows comparison of the energy spectra for the case  $\theta_1 = -\pi/4$ ,  $\theta_2 = \pi/4$  calculated by using the technique just described and straightforward plane wave expansion. The two are identical within numerical precision, confirming yet again that simple plane wave expansion generates a solution described by  $\theta_{1(2)} = \pm\pi/4$ .

Quite a different result is obtained for boundary conditions  $\theta_A = 0$ ,  $\theta_B = 0$ . The spectrum in this case is gapped. The symmetry analysis can be applied to describe the spectrum just as in the previous section. Relevant symmetry transformations and the star of equivalent symmetry points are shown in Fig. 7. The features of the numerical results fully agree with the results of numerical calculation: for example the energy bands are symmetric under transformation  $(E, \mathbf{k}) \rightarrow (-E, \mathbf{k})$ , and the segments  $XM$  and  $YG$  are equivalent.

As was pointed out, for general boundary condition even the symmetry  $(E, \mathbf{k}) \rightarrow (-E, \mathbf{k})$  of the single node energy spectrum is absent.

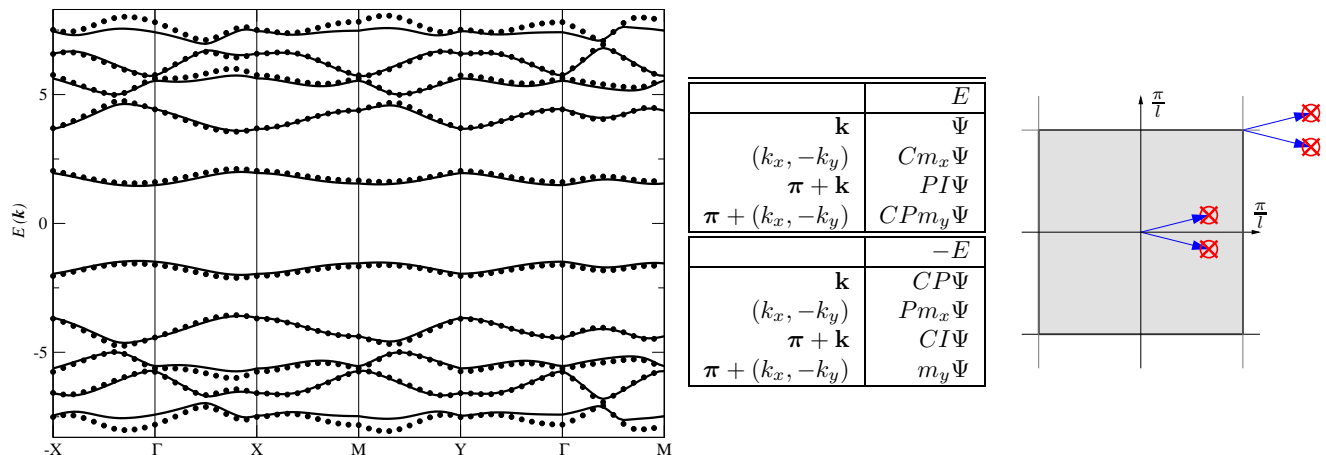


FIG. 7: Left panel: the energy bands of linearized Hamiltonian for two vortices per unit cell and boundary conditions  $\theta_A = \theta_B = 0$ . The spectrum obtained by OPW method is shown by solid lines, the dots represent the spectrum of Hamiltonian (34) with mass  $M(\mathbf{r})$  chosen as Gaussian  $M_0 \exp(-\mathbf{r}^2/\xi^2)$ , centered around each vortex with parameters  $M_0 = 100/l$ ,  $\xi = 0.05l$ . Small discrepancies between the results obtained by two techniques for high energy bands are due to finite size of the core size  $\xi/l$  used in the numerical calculation. Center panel: symmetry operations relating eigenenergies at different  $\mathbf{k}$ . Right panel: the first Brillouin zone with equivalent  $\mathbf{k}$  vectors shown by circles. For every state with energy  $E$  at momentum  $\mathbf{k}$  there is a state with the same momentum and energy  $-E$ .

## VI. RELATION OF THE SINGULAR LINEARIZED HAMILTONIAN TO THE NON-LINEARIZED, REGULAR PROBLEM

As explained in previous sections, the spectrum of linearized Hamiltonian, in which vortices appear as point-like defects, depends on the boundary conditions imposed at vortex locations. These boundary conditions are in turn determined by the self-adjoint extension of the linearized model. In principle, in order to establish which particular self-adjoint extension should be used, one faces solving the original, fully self-consistent BdG equations, a project beyond the scope of the present paper.

Still, in the simplest case of a  $d$ -wave superconductor with no additional forms of ordering in the interior of vortex cores, the physics of nodal quasiparticles should be adequately described by the Hamiltonian of Eq. (2) and we should be able to say something definite about the meaning of different self-adjoint extensions. A useful perspective on various choices of boundary conditions, i.e. various choices of the parameter  $\theta$ , can be gained by noticing that the main feature of the self-consistent solution is to suppress the quasiparticle wavefunctions inside vortex cores. Furthermore, such fully self-consistent solution does not require any additional boundary conditions at vortex locations, since non-linear terms, which grow strongly near vortices, and the self-consistency condition conspire to regularize the wavefunctions inside the core.

How can such behavior be emulated on the level of a Dirac Hamiltonian *without* explicitly enforcing the boundary conditions? Unlike particles described by a Schrödinger Hamiltonian, Dirac fermions cannot be prevented from penetrating vortex cores by a strong scalar

potential barrier at vortex locations – if such a barrier is imposed it leads to the Klein paradox<sup>48</sup>. The correct procedure which ensures suppression of the Dirac spinor amplitude in a particular region of space requires that the mass of the particle be treated as a function of position  $M(\mathbf{r})$ , so that in the prohibited region such mass becomes very large<sup>48</sup>. If the mass of the particle in the interior of forbidden region is set to  $M_0$ , then the spinor wavefunctions experience an exponential suppression in this same region, with a penetration length  $\sim 1/M_0$ . In order to regularize the FT Hamiltonian by requiring suppression of the nodal quasiparticle wavefunctions inside vortex cores, we are thus led to introduce a short-ranged mass-like potential  $\sigma_2 M(\mathbf{r})$  that vanishes at distances larger than the core size  $\sim \xi$ . Inside the core, the absolute value of mass  $M_0$  should be chosen to be much larger than  $1/\xi$ .

Even in the zero-field problem such mass term breaks time-reversal symmetry:  $\sigma_2 M(\mathbf{r})$  changes sign under the time-reversal operation, and one might expect that in such terms in general lead to opening of a gap in the spectrum. The detailed analysis shows that FT equations augmented by mass potentials

$$\frac{1}{v_F} \mathcal{H}'_{FT} = (p_x + a_x)\sigma_3 + \alpha_{\Delta}\sigma_1(p_y + a_y) + v_x + \sigma_2 M(\mathbf{r}) \quad (34)$$

are generally *not* invariant under symmetry operations listed in Table III from Appendix. The transformation properties of the mass term itself  $M(\mathbf{r})$  are shown in Table II. Clearly, *no* choice of nonzero mass term  $M(\mathbf{r})$  is invariant under *all* symmetry operations, just as no choice of  $\theta_i$ 's preserves *all* the symmetries of  $H_{FT}$ . For  $M(\mathbf{r})$  possessing certain specific symmetries, some of the

1	$I$	$P$	$PI$
$M(\mathbf{r})$	$-M(I\mathbf{r})$	$-M(P\mathbf{r})$	$M(\mathbf{s}\mathbf{r})$
$C$	$CI$	$CP$	$CPI$
$-M(\mathbf{r})$	$M(I\mathbf{r})$	$M(P\mathbf{r})$	$-M(\mathbf{s}\mathbf{r})$

TABLE II: Transformation of the position-dependent mass term  $M(\mathbf{r})$  under operations commuting with  $H_{FT}$ . Only for  $M(\mathbf{r})$  of special symmetries the new Hamiltonian  $H'_{FT} = H_{FT} + \sigma_2 v_F M(\mathbf{r})$  remains invariant upon the action of these operations.

transformations do commute with the Hamiltonian. For example, if the mass does not change under inversion about a vortex and has the same sign for all vortices:

$$M(I\mathbf{r}) = M(\mathbf{r}) = M(\mathbf{s}\mathbf{r}),$$

then the transformations commuting with the Hamiltonian coincide with those listed in Fig. 7. Thus the Hamiltonian with such mass terms is *equivalent* to the original FT Hamiltonian with  $\theta_1 = \theta_2 = 0$  and with mass equal to zero. The spectrum of  $\mathcal{H}'_{FT}$  calculated by the standard plane wave expansion is shown in Fig. 7 and agrees with the numerical results based on the OPW method. Similarly, a straightforward calculation shows that the choice of

$$M(\mathbf{r}) = M(I\mathbf{r}) = -M(P\mathbf{r})$$

corresponds to  $\theta_1 = 0$ ;  $\theta_2 = \pi/2$ , while

$$M(\mathbf{r}) = -M(I\mathbf{r}) = -M(P\mathbf{r})$$

describes  $\theta_1 = -\theta_2 = \pi/4$ . The latter choice requires that  $M(\mathbf{r})$  has a  $p$ -wave symmetry and vanishes at least along two directions around each vortex. This choice also illustrates the following important point: while the mass term always breaks time-reversal symmetry, in the  $\theta_1 = -\theta_2 = \pi/4$  case it does so only *locally* while leaving this symmetry intact on *average* since  $\int d^2r M(\mathbf{r}) = 0$ . Here the integration is over the small region within which  $M(\mathbf{r})$  differs appreciably from zero around a *single* vortex.

We will conclude this section with two observations. First, if the overall amplitude of the mass term is increased continuously, then the gap in the spectrum will also increase, and it is not *a priori* clear that in the limit of extremely small magnetic field the magnitude of the gap induced by the mass term is proportional to  $1/l$  rather than  $1/l^2$ . To answer that question we note that if the absolute value of the mass  $M(\mathbf{r})$  inside vortex core is denoted as  $M_0$ , then the quasiparticles penetrate into the vortex core to distances of order  $1/M_0$ . Since the distance should be much smaller than the size of the vortex core  $\xi$ , we find that  $M_0 \gg l/\xi$ . The scaling limit, therefore is obtained as a limit of infinite  $M_0$ .

Our analysis does not allow us to uniquely determine which self-adjoint extension (specified by  $\theta_{1,2}$  or by symmetry of the mass terms) is realized in cuprates, as the

answer depends significantly on short range physics and can be determined only through the detailed analysis of the spectrum and the wavefunctions of self-consistent solution. However, given the extension of the Hamiltonian describing quasiparticles near node 1, the symmetry properties of the full BdG Hamiltonian determine unambiguously the self-adjoint extensions of linearized Hamiltonian near nodes  $\bar{1}$ , 2 and  $\bar{2}$ .

Symmetry operations of the linearized Hamiltonian listed in (Table III in the Appendix) also commute with the full BdG Hamiltonian  $\mathcal{H}$  defined by (5), where now these symmetry operations are applied to the full wavefunction  $\Psi$ . One should note, however, that these operation have entirely different meaning as  $\mathcal{H}$  describes simultaneously all four nodes and most of the operations relate the eigenstates belonging to different nodes. For example, the action of the inversion operator on an eigenfunction  $\Psi(\mathbf{r})$  of  $\mathcal{H}$  will now be understood as  $\Psi(-\mathbf{r})$ :

$$\Psi(\mathbf{r}) \approx e^{ik_F x} \psi(\mathbf{r}) \rightarrow e^{-ik_F x} \psi(-\mathbf{r});$$

the reader should compare this to the ‘‘inversion’’ operation of Eq. (25). Thus, it transforms the state near node 1 into a state with Fourier components localized in the vicinity of  $\bar{1}$ . Similarly, symmetry operations involving reflections  $m_x$  and  $m_y$  applied to quasiparticle wavefunctions with Fourier components localized near node 1, generate new wavefunctions near nodes 2 and  $\bar{2}$ .

For simplicity, we will focus on transformations generated by  $P$ ,  $I$ , and  $C$ , which relate nodes 1 and  $\bar{1}$  only. Acting on a wavefunction  $\psi(\mathbf{r})$  with crystal momentum  $\mathbf{k}$  and energy  $E$ , they generate seven new states shown schematically in Fig. 8.

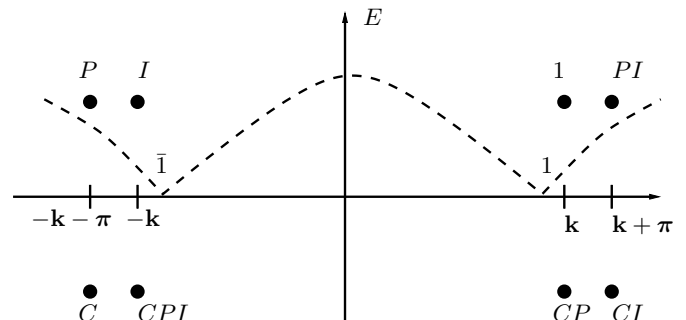


FIG. 8: Symmetry of the spectrum for the full BdG Hamiltonian  $\mathcal{H}$ .

Note that transformations  $PI$ ,  $CP$ , and  $CI$  relate wavefunctions near the same node. They ensure that if  $\Psi(\mathbf{r})$  is an eigenstate of Hamiltonian (2) with energy  $E$  and momentum  $\mathbf{k}$  then the spectrum of  $\mathcal{H}$  also has states characterized by  $(\mathbf{k}, -E)$ ,  $(\mathbf{k} + \boldsymbol{\pi}, E)$ , and  $(\mathbf{k} + \boldsymbol{\pi}, -E)$ .

One can easily verify that there are only two self-adjoint extensions compatible with  $PI$ ,  $CI$  and  $CP$ :  $\theta_1 = \theta_2 = 0$  and  $\theta_1 = \theta_2 = \pi/2$ . The two choices are essentially equivalent being related to each other by reflection  $m_x$ . The resulting single-node energy spectrum



is shown in (7). It is characterized by strongly dispersive bands at low energies, except for the lowest gapped narrow bands at energies  $\approx \pm 2\hbar v_F/l$ .

All other boundary conditions break one of the three symmetries. In particular, if the spectrum is gapless at  $\mathbf{k}_1^F$  then it should also be gapless at momentum  $\mathbf{k}_1^F + \boldsymbol{\pi}$ . This is clearly not the case for the choice  $\theta_1 = \pi/4$ ,  $\theta_2 = -\pi/4$  shown in Fig. 5. To restore the full symmetry of the non-linearized BdG Hamiltonian (2), one has to demand that the linearized version is a *union* of two independent self-adjoint extensions:  $\theta_1 = -\theta_2 = \pi/4$  and  $\theta_1 = -\theta_2 = -\pi/4$ . Such union is a combination of the solution found in Ref. 8 and its companion solution with the A and B labels interchanged (DOS, of course, remains unaffected apart from a mere factor of two). Consequently, the single-node linearization corresponds to *two independent* problems described by the same Hamiltonian operator, but with different boundary conditions near vortices. Under *PI* operation, the Hilbert spaces of the two Hamiltonians are interchanged and the full symmetry is thereby restored. Observe that this is a deeply non-perturbative result: such a union describes *eight* two-component Dirac fermions and therefore 16 zero energy states at BdG nodes, in contrast to only four massless Dirac fermions of the  $H = 0$  case. Recent exact symmetry arguments on a tight-binding lattice<sup>70</sup>, based on a form of the index theorem, strongly support the identification of the above union as the proper self-adjoint extension of the continuum linearized problem with gapless spectrum.

## VII. LINEARIZATION OF $d_{x^2-y^2}$ HAMILTONIAN

In the companion paper<sup>47</sup>, we consider properties of a tight-binding lattice  $d$ -wave superconductor in the mixed state. The simplest representative of such systems is characterized by the  $d_{x^2-y^2}$  symmetry of the order parameter rather than the  $d_{xy}$  case considered in previous sections. In order to directly compare the linearized model and the tight-binding lattice model, we use this section to consider the linearized Hamiltonian with the “clover” of the  $d$ -wave gap function rotated by 45 degrees with respect to the vortex lattice. After following the standard steps<sup>10,47</sup>, we find that the linearized Hamiltonian in this case is given by

$$H_{x^2-y^2}^{lin} = v_F \frac{\Pi_x + \Pi_y}{\sqrt{2}} \sigma_3 + v_\Delta \frac{\Pi_y - \Pi_x}{\sqrt{2}} \sigma_1 + v_F \frac{v_x + v_y}{\sqrt{2}} \quad (35)$$

where  $\Pi_i = p_i + a_i$  is the generalized momentum. In the rest of the section, we consider the properties of the above Hamiltonian for precisely the same orientation and position of the vortex lattice as before, with the unit cell shown in Fig. 1. Therefore, the potentials  $\mathbf{v}$  and  $\mathbf{a}$  remain exactly the same, and the only difference from the original Hamiltonian  $\mathcal{H}_{FT}$  is the direction of the  $d$ -wave nodes relative to the vortex lattice.

As before, we will confine ourselves to the isotropic case  $v_F = v_\Delta$ . Note that in this case, if one neglects the superfluid velocity terms and retains only the vector potential  $\mathbf{a}$ , Hamiltonians  $H_{x^2-y^2}^{lin}$  and  $H_{FT} \equiv H_{xy}^{lin}$  are related by a unitary SU(2) transformation  $U = \exp(i\sigma_y\pi/8)$ . Therefore, both are expected to have the same density of states. Moreover, since this unitary transformation is global, the dispersions  $E_n(\mathbf{k})$  of the two cases will also be identical.

The above invariance is a consequence of the combination of our Dirac particles effectively being at  $\mathbf{k} = 0$  and the axially-symmetric character of the free Dirac problem. Since there is no preferred direction for the free Dirac problem, different orientation of the vortex lattice cannot change the spectrum. This invariance, of course, holds for any linearized Hamiltonian with an arbitrary direction of the  $d$ -wave “clover”. The unitary transformation in this general case, relating the Hamiltonian to  $H_{FT}$  is  $U = \exp(i\sigma_y\alpha/2)$ , where  $\alpha$  is the direction of the node relative to  $x$ -axis.

Of course, this invariance is violated by the superfluid velocity terms and finite anisotropy. In the latter case, there *is* a preferred direction since the free Dirac dispersion defines an elongated cone. Similarly, the terms containing the superfluid velocity  $\mathbf{v}$  carry the information about a particular direction of the node, where the linearization is performed, and therefore break the rotational symmetry, even when  $\mathbf{a}$  is set to zero. Numerically, the effects of  $\mathbf{v}$  turn out to be rather small at the lowest band energies, and become progressively more important for higher bands. Fig. 9 shows the spectrum of  $d_{x^2-y^2}$  superconductor obtained numerically using a simple expansion in plane waves. For the lowest bands, it is very similar to the spectrum of  $d_{xy}$ -superconductor discussed in detail in the earlier sections (see Fig. 5). In both  $d_{xy}$  and  $d_{x^2-y^2}$  cases, for the lowest band the result is very close to that of the reduced Hamiltonian, which contains only the vector potential  $\mathbf{a}$  – the effect of the scalar potential becomes pronounced only at higher energies. The spectrum of the Hamiltonian with only the scalar potential  $\mathbf{v}$  included and the vector potential set to zero by hand, is quite different – at low energies it is a tiny perturbation of the free Dirac dispersion. This is in stark contrast with the result of the so-called “Volovik approximation.”<sup>4</sup>

The allowed class of the boundary conditions near vortices for  $H_{x^2-y^2}^{lin}$  can be obtained directly from the boundary conditions of the  $d_{xy}$  case (22) and (23) by noting that in the coordinate system  $(x', y')$  rotated by 45 degrees with respect to  $(x, y)$ ,  $H_{x^2-y^2}^{lin}$  takes on the form identical to  $H_{FT}$ , except for the vortex lattice being rotated by  $\pi/4$  relative to what it used to be in the  $d_{xy}$  case. Still, when deriving the asymptotics of the wavefunctions near a vortex, only the singular terms due to that single vortex contribute – different geometry of the lattice therefore does not directly affect the boundary conditions. All we need to do is to return to the original coordinate system by performing the rotation  $\phi \rightarrow \phi - \pi/4$  in (22) and (23).

The symmetry properties of the Hamiltonian  $H_{x^2-y^2}^{lin}$

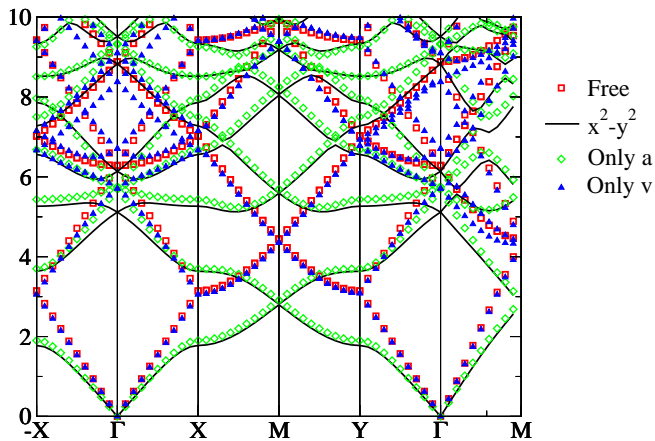


FIG. 9: The quasiparticle spectrum of the mixed state obtained by an expansion of the wavefunctions in the plane wave basis. The dispersion of the zero magnetic field problem is shown in red squares, the dispersion of a  $d_{x^2-y^2}$  superconductor in the presence of a vortex lattice is shown by a solid black line. The green diamonds (blue triangles) correspond to the artificial Hamiltonian, which is obtained by setting the scalar potential  $\mathbf{v}$  (vector potential  $\mathbf{a}$ ) in  $H_{FT}$  to zero. Note that the role of the scalar potential at low energies is small, and that makes the spectrum of  $H_{x^2-y^2}^{lin}$  rather similar to  $H_{xy}^{lin} = H_{FT}$  shown in Fig. 5.

can be derived rather straightforwardly, since  $\mathbf{v}$  and  $\mathbf{a}$  are exactly the same as before, and we can use their properties from Table I. The symmetry properties of the Hamiltonian, which do not involve mirror symmetries, remain exactly the same. Namely, transformations  $I, P, C$  and their combinations can be literally taken from Table III. The transformations involving mirror symmetries are modified, however. Moreover, in addition to the mirror planes along the  $x$  and  $y$  directions, now a new mirror symmetry plane appears along the diagonal of the unit cell. The appearance of these new elements of symmetry is important for a precise form of the spectrum. It is easy to see from Figs. 5 and 9 that, although the spectra of the  $d_{xy}$  and  $d_{x^2-y^2}$  are quite close, the latter is more symmetric due to the additional symmetry  $x \leftrightarrow y$ .

The main conclusions, nevertheless, remain the same. For example, the symmetry of the Hamiltonian operator requires that the spectrum is symmetric under translations in momentum space by  $(\pi/l, \pi/l)$ . In other words, if there is a node at  $\mathbf{k} = 0$ , it should have been replicated at the corner of the unit cell. Clearly, the dispersion of Fig. 9 has only one gapless point at  $\mathbf{k} = 0$ . The reason, just as before, is the necessity of imposing the boundary conditions which again violate the symmetries of what is formally the Hamiltonian operator.

### VIII. CONCLUSIONS

The main results of this paper can be summarized as follows: the linearized BdG Hamiltonian describing

nodal fermions in the mixed state of a  $d_{x^2-y^2}$  superconductor has to be complemented by a set of boundary conditions (22,23) specifying the behavior of quasiparticle wavefunctions near vortices in order for the problem to be mathematically fully defined. The boundary conditions contain a single parameter  $\theta \in [0, \pi)$  for each vortex which cannot be found from within the linearized theory itself, but should be determined from the full non-linearized calculation. All the physics beyond linearization, such as the intervortex scattering and interference effects, particle-hole asymmetry, high energy and curvature terms, etc., is implicitly reflected in the effective linearized FT Hamiltonian *only* through these boundary conditions. Consequently, the linearized FT Hamiltonian actually describes a *family* of distinct self-adjoint extensions reflecting a variety of high-energy processes that might be taking place inside the vortex cores (magnetism, Mott insulator, charge density-wave, etc.). Such multitude of all possible short-range physics behaviors can be classified according to the set of  $\theta$  parameters, which govern different “universality” classes of the nodal fermion quantum “criticality.” The conventional Simon-Lee scaling function must be generalized to include the explicit dependence on  $\theta$ ’s, as explained in the text. Once the boundary conditions are properly imposed according to (22,23), the solutions of the FT equations are fully determined and are independent of the assignment of A or B vortices, thereby restoring their invariance under arbitrary singular gauge transformations.

In earlier work<sup>8</sup> the boundary conditions were not explicitly enforced but instead were “spontaneously” selected by the procedure used to diagonalize the Hamiltonian. Such an expansion in the plane wave basis results in  $\theta_{1(2)} = \pm\pi/4 (\mp\pi/4)$ , which was indeed found here to be the self-adjoint extension appropriate to the nodal gapless behavior of a  $d$ -wave superconductor in the limit of low magnetic fields. In general, however, the boundary conditions  $\theta_{1(2)}$  should be found from the full self-consistent BdG Hamiltonian and serve as an external input to the linearized theory describing the bulk quasiparticle states.

The authors thank Dr. O. Vafeek for useful discussions and Profs. M. R. Zirnbauer and A. Altland for helpful correspondence and for sharing with us their unpublished results. This work was supported in part by the NSF grants DMR-0094981 and DMR-0531159.

### APPENDIX A: SUPERFLUID VELOCITY AND THE PHASE OF SUPERCONDUCTING ORDER PARAMETER

#### 1. Simple properties

For the reference, we summarize the properties of superfluid velocity and the phase of the order parameter used in the text. Consider a periodic lattice of vortices with a basis, with  $N$  vortices located at  $\mathbf{R}_i$  within a

square unit cell of size  $l \times l$  as shown in Fig. 10. The

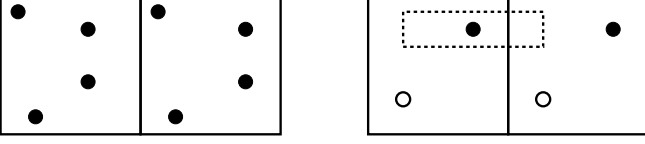


FIG. 10: Left panel: An example of a vortex lattice for the case of  $N=4$  vortices per unit cell. Right panel: Two vortices per unit cell: integral (A17) calculated along the contour shown as a dashed line equals  $2\pi$ .

superfluid velocity is defined as

$$m\mathbf{v} = \frac{1}{2}\hbar\nabla\phi - \frac{e}{c}\mathbf{A} \quad , \quad (\text{A1})$$

where  $\phi(\mathbf{r})$  is the phase of the order parameter. The latter can be determined from the requirement that it acquires  $2\pi$  as  $\mathbf{r}$  encircles a vortex:

$$\nabla \times \nabla\phi = 2\pi\hat{z} \sum_{\mathbf{R}} \delta(\mathbf{r} - \mathbf{R}) \quad , \quad (\text{A2})$$

where  $\mathbf{R}$  denotes the position of the vortices. Since the superfluid velocity typically enters in combination  $m\mathbf{v}$  we will often set  $m = 1$ , for compactness.

Using the Fourier transforms, the superfluid velocity can be written<sup>66</sup> as

$$\mathbf{v}(\mathbf{r}) = i\pi\hbar \int \frac{d^2k}{(2\pi)^2} \frac{\mathbf{k} \times \hat{z}}{\lambda^{-2} + k^2} e^{i\mathbf{k}\cdot\mathbf{r}} \sum_{\mathbf{R}} e^{-i\mathbf{k}\cdot\mathbf{R}} \quad , \quad (\text{A3})$$

where  $\lambda$  is the London penetration length. Let us write the position of a vortex as  $\mathbf{R} = \mathbf{R}_i + \boldsymbol{\tau}$ , where index  $i = 1 \dots N$  labels the vortices inside an arbitrarily chosen reference unit cell, and  $\boldsymbol{\tau} = l(N_x\hat{x} + N_y\hat{y})$  with integer  $N_x, N_y$  denotes lattice translation vectors. Then, after summation over  $\boldsymbol{\tau}$ , the superfluid velocity can be expressed as

$$\mathbf{v}(\mathbf{r}) = \frac{i\pi\hbar}{l^2} \sum_{\mathbf{Q}} \frac{(Q_y, -Q_x)}{Q^2 + \lambda^{-2}} e^{i\mathbf{Q}\cdot\mathbf{r}} \sum_{i=1}^N e^{-i\mathbf{Q}\cdot\mathbf{R}_i} \quad , \quad (\text{A4})$$

where  $\mathbf{Q} = 2\pi(\hat{x}N_x + \hat{y}N_y)/l$  with integer  $N_x, N_y$  are the reciprocal lattice vectors. Note that when  $\lambda \gg l$ , one can neglect  $\lambda^{-2}$  in the denominator in all terms of the sum except for  $\mathbf{Q} = \mathbf{0}$ , and the simplified result reads:

$$\mathbf{v}(\mathbf{r}) = \frac{i\pi\hbar}{l^2} \sum_{\mathbf{Q} \neq \mathbf{0}} \frac{(Q_y, -Q_x)}{Q^2} e^{i\mathbf{Q}\cdot\mathbf{r}} \sum_{i=1}^N e^{-i\mathbf{Q}\cdot\mathbf{R}_i} \quad . \quad (\text{A5})$$

This simplification corresponds to replacing the magnetic field  $H(\mathbf{r})$  by its spatial average, as can be verified directly by comparing  $\nabla \times \mathbf{v}$  from (A4) and (A1). In the rest of the appendix and in the main text, the limit  $\lambda \gg l$  is always implied, and  $A(\mathbf{r})$  denotes the vector potential corresponding to the uniform applied magnetic field,

without including small corrections due to the vortex lattice, which are smaller by a factor of  $l^2/\lambda^2$ .

The superfluid velocity  $\mathbf{v}$  can be expressed in a closed form through Weierstrass elliptic zeta function (see also Ref. 55). To derive this expression, let us start from (A2), and write the phase  $\phi$  as

$$\phi(\mathbf{r}) = \phi_0(\mathbf{r}) + \sum_{\mathbf{R}} \arctan \frac{y - Y}{x - X} \quad ,$$

where  $\phi_0(\mathbf{r})$  is a continuous function to be determined later and the second term is a sum of the polar angles describing  $\mathbf{r}$  with respect to the vortex location  $\mathbf{R}$ . After denoting  $z = x + iy$  and substituting  $\phi$  into (A1) we obtain

$$v_y + iv_x = \sum_{i=1}^N \frac{\hbar}{2} \sum_{\tau} \frac{1}{z - Z_i - \tau} - \frac{e}{c}(A_y + iA_x) + \frac{1}{2}(\nabla_y\phi_0 + i\nabla_x\phi_0) \quad , \quad (\text{A6})$$

where the lattice vectors are  $\tau = \tau_x + i\tau_y$  and the location of the vortices within the reference unit cell are now encoded by  $Z_i = X_i + iY_i$ . The sum over the lattice vectors  $\tau$  in the right hand side differs from the definition of Weierstrass zeta-function

$$\zeta(z) = \frac{1}{z} + \sum_{\tau \neq 0} \left( \frac{1}{z - \tau} + \frac{1}{\tau} + \frac{z}{\tau^2} \right) \quad (\text{A7})$$

only by a presence of the constant and linear in  $z$  terms, which are required to ensure the absolute convergence of the sum (A7). These terms can be absorbed into the ‘‘smooth’’ part of the phase by defining  $\phi'_0 = \phi_0 + C_0z + \frac{1}{2}C_1z^2$ , where  $C_{1,2}$  are appropriately chosen constants. Thus, the superfluid velocity satisfies the following equation:

$$v_y + iv_x = \frac{\hbar}{2} \sum_{i=1}^N \left( \zeta(z - Z_i) - \frac{\pi\hbar\bar{z}}{l^2} \right) + \frac{\nabla_y\phi'_0 + i\nabla_x\phi'_0}{2} \quad . \quad (\text{A8})$$

Here, for convenience we chose the symmetric gauge:

$$\frac{e}{c}\mathbf{A} = \frac{\pi N}{2l^2}(-y, x) \quad .$$

Note now that  $w(x, y) = \nabla_y\phi'_0 + i\nabla_x\phi'_0$  satisfies both Cauchy-Riemann conditions:  $\partial_x(\text{Re}w) = \partial_y(\text{Im}w)$  is satisfied automatically, whereas the second condition  $\partial_y(\text{Re}w) = -\partial_x(\text{Im}w)$  is satisfied due to the requirement  $\text{div } \mathbf{v} = 0$  and (A8). Since  $\phi_0$  (and consequently  $\phi'_0$ ) was chosen as a smooth part of the phase, it is therefore a finite analytic function of  $z$  in the entire complex plane, and by Liouville theorem must be equal to a constant. The remaining constant is fixed by the requirement for the spatial average of  $\mathbf{v}$  to vanish (cf. A5), and the final result, which is equivalent to (A5), reads

$$v_y + iv_x = \frac{\hbar}{2} \sum_{i=1}^N \left( \zeta(z - Z_i) - \pi\hbar \frac{\overline{z - Z_i}}{l^2} \right) \quad . \quad (\text{A9})$$

Note that the superfluid velocity  $\mathbf{v}(\mathbf{r})$  is periodic in space with the same unit cell as the unit cell of the vortex lattice.

## 2. The phase of the order parameter

Unlike the superfluid velocity components, neither the phase of the order parameter  $\phi(\mathbf{r})$ , nor  $\exp(i\phi)$ , and not even  $\nabla\phi$  are periodic, regardless of the gauge used. Since the periodicity of  $\exp(i\phi)$  would have required that  $\nabla\phi$  is itself periodic, it is sufficient to prove the statement for  $\nabla\phi$ : consider a contour integral  $\oint \nabla\phi \cdot d\mathbf{l}$  along the boundaries of the unit cell. Since there are  $N$  vortices inside the contour, the integral must equal  $2\pi N$ . On the other hand, the assumption of  $\nabla\phi$  being periodic would have resulted in vanishing of the integral due to the cancellation between the contributions of the opposite edges.

Although the phase cannot be made periodic, it is quasi-periodic and can be expressed in a closed form through Weierstrass sigma-function  $\sigma(z)$ . Since (A1) yields

$$\partial_y\phi + i\partial_x\phi = \sum_i \left( \zeta(z - Z_i) + \frac{\pi\bar{Z}_i}{l^2} \right) ,$$

the difference  $\phi(\mathbf{r}) - \phi(\mathbf{r}_0)$ , where  $\mathbf{r}_0$  is an arbitrary reference point, can be written as

$$\begin{aligned} \int_{\mathbf{r}_0}^{\mathbf{r}} \nabla\phi \cdot d\mathbf{l} &= \text{Im} \int_{z_0}^z (\partial_y\phi + i\partial_x\phi) dz \\ &= \text{Im} \sum_i \left( \int_{z_0 - Z_i}^{z - Z_i} \zeta(w) dw + \frac{\pi\bar{Z}_i(z - z_0)}{l^2} \right) , \end{aligned} \quad (\text{A10})$$

where the contours in all integrals are assumed to be the same. For different contours, the equality holds modulo  $2\pi$ . Since the Weierstrass sigma-function  $\sigma(z)$  is defined according to  $\sigma'(z)/\sigma(z) = \zeta(z)$ , which implies

$$\ln \frac{\sigma(z)}{\sigma(z_0)} \equiv \int_{z_0}^z \zeta(z) dz \pmod{2\pi} ,$$

the phase  $\phi(\mathbf{r})$  can be written as

$$\begin{aligned} \phi(\mathbf{r}) - \phi(\mathbf{r}_0) &\equiv \sum_i \text{Arg} \frac{\sigma(z - Z_i)}{\sigma(z_0 - Z_i)} \\ &+ \frac{\pi}{l^2} \text{Im} \left( (z - z_0) \sum_i \bar{Z}_i \right) \pmod{2\pi} . \end{aligned} \quad (\text{A11})$$

Since the phase  $\phi(\mathbf{r})$  is defined up to an arbitrary constant, even for a fixed gauge of the vector potential  $\mathbf{A}$ , it is convenient to choose the constant  $\phi(\mathbf{r}_0)$  in such a way that

$$\phi(\mathbf{r}) = \sum_i \text{Arg}[\sigma(z - Z_i)] + \frac{\pi}{l^2} \text{Im} \left( z \sum_i \bar{Z}_i \right) \pmod{2\pi} . \quad (\text{A12})$$

Eq-n (A12) is the explicit expression for the phase  $\phi(\mathbf{r})$  used in the main text and in the rest of the appendix.

## 3. Two vortices per unit cell

In general, the procedure of separation of the phase  $\phi(\mathbf{r})$  into  $\phi_A$  and  $\phi_B$  is straightforward by using (A12). In this section we illustrate it for the simplest case of  $N = 2$  with two vortices located at  $\mathbf{R}_A$  and  $\mathbf{R}_B$  inside an arbitrary reference unit cell of size  $l \times l$  (see Fig.1). The vector potential in the symmetric gauge is given by

$$\frac{e}{c} \mathbf{A} = \frac{\pi}{l^2} (-y, x) ,$$

and the velocities  $\mathbf{v}_{A,B}$  can be defined similarly to  $\mathbf{v}$ :

$$\mathbf{v}_{A(B)}(\mathbf{r}) = \frac{2i\pi\hbar}{l^2} \sum_{\mathbf{Q} \neq 0} \frac{(Q_y, -Q_x)}{Q^2} e^{i\mathbf{Q}\mathbf{r}} e^{-i\mathbf{Q}\mathbf{R}_{A(B)}} . \quad (\text{A13})$$

Clearly,  $\mathbf{v}_{A(B)}$  automatically satisfy  $\mathbf{v}_A + \mathbf{v}_B = 2\mathbf{v}$  (see (A3)). Moreover, since  $\mathbf{v}_{A(B)}/2$  is formally given by the same Fourier expansion as  $\mathbf{v}$  for  $N = 1$  (cf. (A3)), we have

$$\frac{\mathbf{v}_{A(B)}}{2} = \frac{1}{2} \nabla\phi_{A(B)} - \frac{e}{2c} \mathbf{A} . \quad (\text{A14})$$

where  $\phi_{A(B)}$  satisfies the analogue of (A2):

$$\nabla \times \nabla\phi_{A(B)} = 2\pi\hat{z} \sum_{\tau} \delta(\mathbf{r} - \mathbf{R}_{A(B)} - \tau) , \quad (\text{A15})$$

The closed form expressions for  $\mathbf{v}_{A(B)}$  can be read off directly from the formulae of the previous section. After defining

$$\begin{aligned} F(\mathbf{r}) &= \text{Arg}[\sigma(x + iy)] \\ \mathbf{Z}(\mathbf{r}) &= \left( \text{Im}\zeta(z) + \frac{\pi y}{l^2}, \text{Re}\zeta(z) - \frac{\pi x}{l^2} \right) , \end{aligned}$$

where  $\sigma(z)$  and  $\zeta(z)$  are Weierstrass functions with periods  $(l, il)$ , the superfluid velocities are simply  $\mathbf{v}_{A(B)} = \mathbf{Z}(\mathbf{r} - \mathbf{R}_{A(B)})$ . The phases  $\phi_{A(B)}$  are given by

$$\phi_{A(B)}(\mathbf{r}) = F(\mathbf{r} - \mathbf{R}_{A(B)}) + \frac{e}{c} \mathbf{A}(\mathbf{R}_{A(B)}) \cdot \mathbf{r} ; \quad (\text{A16})$$

by construction they obey the condition  $\phi_A(\mathbf{r}) + \phi_B(\mathbf{r}) = \phi(\mathbf{r})$ .

In our discussion of the quasiparticle spectrum, we use the symmetry properties of the phase difference  $\delta\phi = \phi_A(\mathbf{r}) - \phi_B(\mathbf{r})$ . Let us show that after a translation by the primitive lattice vector  $l\hat{x}$ , the phase difference acquires a  $\pi$ -shift. Consider the following integral along a straight line connecting  $\mathbf{r}$  and  $\mathbf{r} + l\hat{x}$ :

$$I(\mathbf{r}) = \int_{\mathbf{r}}^{\mathbf{r} + l\hat{x}} (\mathbf{v}_A - \mathbf{v}_B) \cdot d\mathbf{l} .$$

Functions  $\mathbf{v}_{A(B)}$  are periodic in unit cell and therefore  $I(x, y)$  does not depend on  $x$ :

$$I(\mathbf{r}) = \int_0^l [\mathbf{v}_A(\xi, y) - \mathbf{v}_B(\xi, y)] d\xi .$$

Next, we note that the contour integral along the path shown in Fig.10 is a multiple of  $2\pi$ :

$$\oint (\mathbf{v}_A - \mathbf{v}_B) \cdot d\mathbf{l} = \oint (\nabla\phi_A - \nabla\phi_B) \cdot d\mathbf{l} = 2\pi(n_A - n_B) , \quad (\text{A17})$$

where the  $n_A - n_B$  is the difference between the number of  $A$  and  $B$  vortices inside the contour. Since the integral along the vertical edges vanishes due to the periodicity of superfluid velocities  $\mathbf{v}_{A(B)}$ , we find that

$$I(x, y_1) - I(x, y_2) = 2\pi n .$$

Choosing  $y_1$  and  $y_2$  so that the horizontal segments are symmetrically located around vortex  $A$  as shown in Fig.10, we have  $I(x, y_1) = -I(x, y_2)$  which yields  $I(x, y_1) = \pi$ , and consequently,

$$\delta\phi(\mathbf{r} + l\hat{x}) - \delta\phi(\mathbf{r}) \equiv \pi \pmod{2\pi} . \quad (\text{A18})$$

Combining this result with a similar identity for the translations in  $y$ -direction:

$$\delta\phi(\mathbf{r} + l\hat{y}) - \delta\phi(\mathbf{r}) \equiv \pi \pmod{2\pi} .$$

we find that  $\exp(i\delta\phi(\mathbf{r}))$  can be written as a product of  $\exp(i\pi(x+y)/l)$  and a periodic function with a unit cell  $l \times l$ .

Other useful identities involving  $\delta\phi = \phi_A - \phi_B$  are

$$\delta\phi(x, y) + \delta\phi(l/2 - x, y) = \pi/2 , \quad (\text{A19})$$

$$\delta\phi(x, y) + \delta\phi(x, l/2 - y) = -\pi/2 , \quad (\text{A20})$$

$$\delta\phi(x, y) + \delta\phi(-x, -y) = 0 . \quad (\text{A21})$$

## APPENDIX B: TWO AHARONOV-BOHM FLUXES – EXACT SOLUTIONS

### 1. Elliptic coordinates and Mathieu functions

In this appendix, we analyze the properties of a two-component Dirac particle moving in the field of two Aharonov-Bohm fluxes. We will prove that the exact solution of the problem is not unique and depends on boundary conditions imposed near the fluxes. To achieve this goal, we first derive a method allowing us to construct exact solutions for the problem of a *Schrödinger* particle in the field of two Aharonov-Bohm solenoids, which carry arbitrary fractional fluxes  $\alpha\phi_0$  and  $\beta\phi_0$ , with  $\phi_0 = hc/e$ . We illustrate our procedure by analyzing several simple, physically interesting examples with  $\alpha, \beta = \pm\frac{1}{2}$ . After solving several model problems for a Schrödinger particle in the field of two fluxes, we apply

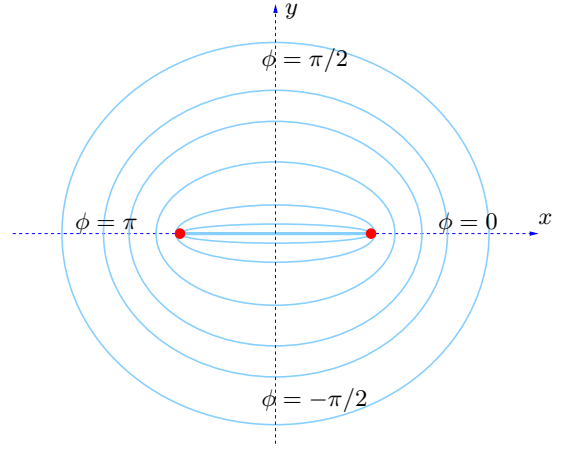


FIG. 11: Elliptic coordinate system. Each line of constant  $z$  is an ellipse. At  $z = 0$  the ellipse is reduced to a segment  $(-a, a)$  of the real axis.

the technique to the case of two-component *Dirac* particles.

In what follows, we will extensively use Mathieu functions. Therefore, we start by reminding the reader of some of their essential properties: the details can be found in Refs. 71, 72, and 73. Mathieu functions appear naturally as solutions of problems possessing elliptical symmetry and expressed in elliptical coordinates. The most common examples are Laplace and Helmholtz equations with boundary conditions specified on an ellipse. The elliptic coordinates are defined according to

$$x = a \cosh z \cos \phi , \quad (\text{B1})$$

$$y = a \sinh z \sin \phi , \quad (\text{B2})$$

where  $a$  is a constant. Points with  $z = 0$  lie on a segment  $(-a, a)$  traversed twice when  $\phi$  is increased from 0 to  $2\pi$ : first from  $+a$  to  $-a$ , and then backwards. For finite  $z$  the contours  $z = \text{const}$  are ellipses (see Fig.11):

$$\frac{x^2}{a^2 \cosh^2 z} + \frac{y^2}{a^2 \sinh^2 z} = 1 ,$$

and angular coordinate  $\phi$  is used to unambiguously specify the position of the point on the ellipse of constant  $z$ . Each ellipse is described by a major and minor semi-axes of lengths  $a \cosh z$  and  $a \sinh z$  respectively. The linear eccentricity defined as the distance from the center to either focus, is the same for the entire family of ellipses and equals  $a$ . At large distances  $r \gg a$ , the contours of constant  $z$  reduce to circles, and the elliptic coordinates effectively reduce to the ordinary polar coordinates  $(\ln \rho, \theta)$ . Both the Poisson and Helmholtz equations are separable in these coordinates – this is why the elliptic coordinate system is useful in various problems of mathematical physics in the first place. The Laplacian in elliptic coordinates assumes the following form:

$$\frac{\partial^2}{\partial x^2} + \frac{\partial^2}{\partial y^2} = \frac{2}{a^2(\cosh 2z - \cos 2\phi)} \left( \frac{\partial^2}{\partial z^2} + \frac{\partial^2}{\partial \phi^2} \right) ,$$

$g$	$\Psi' = D(g)\Psi$	$E'$	$\mathbf{k}'$	$\theta'_{1(2)}$
1	$\Psi(\mathbf{r})$	$E$ ,	$\mathbf{k}$	$\theta_{1(2)}$
$m_x$	$e^{-i\delta\phi}\sigma_1\Psi(g\mathbf{r})$	$E$ ,	$\boldsymbol{\pi} + (-k_x, k_y)$	$\pi/2 + \theta_{1(2)}$
$m_y$	$e^{-i\delta\phi}\sigma_1\Psi(g\mathbf{r})$	$-E$ ,	$\boldsymbol{\pi} + (k_x, -k_y)$	$\pi - \theta_{1(2)}$
$I$	$\Psi(g\mathbf{r})$	$-E$ ,	$-\mathbf{k}$	$\pi/2 - \theta_{1(2)}$
$P$	$e^{-i\delta\phi}\Psi(g\mathbf{r})$	$-E$ ,	$\boldsymbol{\pi} - \mathbf{k}$	$\pi/2 - \theta_{2(1)}$
$Pm_x$	$\sigma_1\Psi(g\mathbf{r})$	$-E$ ,	$(k_x, -k_y)$	$-\theta_{2(1)}$
$Pm_y$	$\sigma_1\Psi(g\mathbf{r})$	$E$ ,	$(-k_x, k_y)$	$\pi/2 + \theta_{2(1)}$
$PI$	$e^{-i\delta\phi}\Psi(g\mathbf{r})$	$E$ ,	$\boldsymbol{\pi} + \mathbf{k}$	$\theta_{2(1)}$

(a)

$Cg$	$D(Cg)\Psi = \Psi'$	$E'$	$\mathbf{k}'$	$\theta'_{1(2)}$
$C$	$e^{-i\delta\phi}\sigma_2\bar{\Psi}(\mathbf{r})$	$E$ ,	$\boldsymbol{\pi} - \mathbf{k}$	$\pi/2 + \theta_{1(2)}$
$Cm_x$	$\sigma_3\bar{\Psi}(g\mathbf{r})$	$E$ ,	$(k_x, -k_y)$	$\theta_{1(2)}$
$Cm_y$	$\sigma_3\bar{\Psi}(g\mathbf{r})$	$-E$ ,	$(-k_x, k_y)$	$\pi/2 - \theta_{1(2)}$
$CI$	$e^{-i\delta\phi}\sigma_2\bar{\Psi}(g\mathbf{r})$	$-E$ ,	$\boldsymbol{\pi} + \mathbf{k}$	$-\theta_{1(2)}$
$CP$	$\sigma_2\bar{\Psi}(g\mathbf{r})$	$-E$ ,	$\mathbf{k}$	$-\theta_{2(1)}$
$CPm_x$	$e^{-i\delta\phi}\sigma_3\bar{\Psi}(g\mathbf{r})$	$-E$ ,	$\boldsymbol{\pi} + (-k_x, k_y)$	$\pi/2 - \theta_{2(1)}$
$CPm_y$	$e^{-i\delta\phi}\sigma_3\bar{\Psi}(g\mathbf{r})$	$E$ ,	$\boldsymbol{\pi} + (k_x, -k_y)$	$\theta_{2(1)}$
$CPI$	$\sigma_2\bar{\Psi}(g\mathbf{r})$	$E$ ,	$-\mathbf{k}$	$\pi/2 + \theta_{2(1)}$

(b)

TABLE III: Transformation of the wavefunctions and the self-adjoint extensions under various symmetry operations. The right column contains operations involving complex conjugation.

and the Helmholtz equation  $\nabla^2 f + k^2 f = 0$  becomes

$$\left( \frac{\partial^2}{\partial z^2} + \frac{\partial^2}{\partial \phi^2} \right) f + \frac{a^2 k^2}{2} (\cosh 2z - \cos 2\phi) f = 0 .$$

After separation of variables via  $f = F(z)G(\phi)$ , one obtains

$$\frac{1}{F(z)} \frac{d^2 F}{dz^2} + \frac{1}{G(\phi)} \frac{d^2 G}{d\phi^2} + \frac{a^2 k^2}{2} (\cosh 2z - \cos 2\phi) = 0 ,$$

which results in

$$\frac{1}{F(z)} \frac{d^2 F}{dz^2} + \frac{a^2 k^2}{2} \cosh 2z = A , \quad (\text{B3})$$

$$\frac{1}{G(\phi)} \frac{d^2 G}{d\phi^2} - \frac{a^2 k^2}{2} \cos 2\phi = -A , \quad (\text{B4})$$

where  $A$  is the separation constant. The conventional form of these equations, which of course must be solved simultaneously for the same constant  $A$ , is

$$\frac{d^2 G}{d\phi^2} + (A - 2q \cos 2\phi) G(\phi) = 0 , \quad (\text{B5})$$

$$\frac{d^2 F}{dz^2} - (A - 2q \cosh 2z) F(z) = 0 , \quad (\text{B6})$$

where  $q$  is a parameter defined as  $q = a^2 k^2 / 4$ .

#### a. Mathieu functions

Since the solutions must be single-valued functions,  $G(\phi)$  must be  $2\pi$ -periodic. This condition restricts  $A$  to a discrete set of so-called characteristic values, which is traditionally written as a union of two subsets representing solutions that are even or odd under transformation  $\phi \rightarrow -\phi$ :

$$\begin{cases} a_0, a_1, a_2, a_3, \dots & \text{(even solutions)} \\ b_1, b_2, b_3, \dots & \text{(odd solutions)} \end{cases} .$$

While working with the elliptic coordinates, it is useful to keep in mind similarities and distinctions from the polar coordinate system. In the latter, the equation for the angular component assumes a form  $G'' + AG = 0$ , and the requirement of  $2\pi$ -periodicity restricts  $A$  to a set of  $m^2$  with integer  $m$ , irrespectively of  $k$ . In the elliptic case, this no longer holds, and the characteristic values  $a_j, b_j$  depend on  $q = a^2 k^2 / 4$ .

For  $A = a_n$  the periodic solution of the equation for  $G(\phi)$  is an even function of  $\phi$ , which is denoted as  $ce_n(\phi, q)$ ,  $n = 0, 1, 2, \dots$ . The odd solutions, occurring for  $A = b_n$ , are denoted as  $se_n(\phi, q)$ . Functions  $ce_n$  and  $se_n$  are known as Mathieu functions, the notation is to remind us that they reduce to  $\cos(n\phi)$  and  $\sin(n\phi)$  respectively in the limit  $q \rightarrow 0$ .

The equation for  $G$  is of second order, so for a given  $A = a_n$  (or  $A = b_n$ ) there is a second independent solution, in addition to  $ce_n(\phi, q)$  (or  $se_n(\phi, q)$ ). However, the second solution of the angular equation is *never* periodic, and therefore it is of limited, if any, importance in applications. The characteristic values  $a_n, b_n$ , as well as the Mathieu functions  $ce_n$  and  $se_n$  are tabulated and well studied, see for example Ref. 71. Finally, we note that Mathieu functions  $\{ce_n(\phi, q), se_n(\phi, q)\}$  form a complete set in the interval  $(0, 2\pi)$  and satisfy the following orthonormality relations:

$$\int_0^{2\pi} ce_n(\phi, q) ce_m(\phi, q) d\phi = \delta_{nm} , \quad (\text{B7})$$

$$\int_0^{2\pi} se_n(\phi, q) se_m(\phi, q) d\phi = \delta_{nm} , \quad (\text{B8})$$

$$\int_0^{2\pi} ce_n(\phi, q) se_m(\phi, q) d\phi = 0 . \quad (\text{B9})$$

#### b. Modified Mathieu functions

Now we turn to the equation (B6) describing the ‘‘radial’’ part of the solutions. Since (B6) and (B5) must be solved simultaneously for the same value of parameter  $A$ , we are interested in solutions of (B6) only for

A	1st solution	$f(0, q)$	$\partial_z f(0, q)$
$a_n$	$Ce_n(z, q) \propto Mc^{(1)}(z, q) \propto Je_n(z, q)$	$\neq 0$	0
$b_n$	$Se_n(z, q) \propto Ms^{(1)}(z, q) \propto Jo_n(z, q)$	0	$\neq 0$
A	2nd solution	$f(0, q)$	$\partial_z f(0, q)$
$a_n$	$Fey_n(z, q) \propto Mc^{(2)}(z, q) \propto Ne_n(z, q)$	$\neq 0$	$\neq 0$
$b_n$	$Ge_y_n(z, q) \propto Ms^{(2)}(z, q) \propto No_n(z, q)$	$\neq 0$	$\neq 0$

TABLE IV: Modified Mathieu functions: notation and values at  $z = 0$ .

$Je_{2n}(z, q)$	$\approx p_{2n}\gamma e^{-z/2} \sin(\sqrt{q}e^z + \frac{\pi}{4})$
$Ne_{2n}(z, q)$	$\approx -p_{2n}\gamma e^{-z/2} \cos(\sqrt{q}e^z + \frac{\pi}{4})$
$Je_{2n+1}(z, q)$	$\approx -p_{2n+1}\gamma e^{-z/2} \cos(\sqrt{q}e^z + \frac{\pi}{4})$
$Ne_{2n+1}(z, q)$	$\approx -p_{2n+1}\gamma e^{-z/2} \sin(\sqrt{q}e^z + \frac{\pi}{4})$
$Jo_{2n}(z, q)$	$\approx s_{2n}\gamma e^{-z/2} \sin(\sqrt{q}e^z + \frac{\pi}{4})$
$No_{2n}(z, q)$	$\approx -s_{2n}\gamma e^{-z/2} \cos(\sqrt{q}e^z + \frac{\pi}{4})$
$Jo_{2n+1}(z, q)$	$\approx -s_{2n+1}\gamma e^{-z/2} \cos(\sqrt{q}e^z + \frac{\pi}{4})$
$No_{2n+1}(z, q)$	$\approx -s_{2n+1}\gamma e^{-z/2} \sin(\sqrt{q}e^z + \frac{\pi}{4})$

TABLE V: Asymptotic expressions for Modified Mathieu functions for  $z \gg 1$  in terms of  $\gamma = 2^{1/2}(\pi^2 q)^{-1/4}$  and the standard coefficients  $p_n$  and  $s_n$  (see Ref. 71).

$A = a_n$  or  $b_n$ . These solutions are known as Modified Mathieu functions. For every value of parameter  $A$  there are two linearly independent solutions: for  $A = a_n$  these solutions are denoted as  $Je_n(z, q)$  and  $Ne_n(z, q)$ , and for  $A = b_n$  the solutions are  $Jo_n(z, q)$  and  $No_n(z, q)$ . These functions take place of Bessel  $J_m(r)$  and Neumann  $N_m(r)$  functions in the more familiar case of polar coordinates; the letters “e” and “o” stand for “odd” and “even” respectively.

Unfortunately the notation used for Modified Mathieu functions is not standardized, and for convenience we provide the Table IV, which relates notations used by different authors. The functions of the first kind,  $Je_n(z, q)$ ,  $Jo(z, q)$ , are proportional to the Mathieu functions of imaginary argument  $ce_n(iz, q)$  and  $se(iz, q)$ . In our subsequent analysis, we will also use the properties of the Modified Mathieu functions at  $z = 0$  and  $z \gg 1$ , which are summarized in the right two columns of Table IV and Table V respectively. In the most general case, the solution of the Helmholtz equation can be written in the following form:

$$f = \sum_{n=0} ce_n(\phi, q) \left( \alpha_n Je_n(z, q) + \beta_n Ne_n(z, q) \right) + \sum_{n=1} se_n(\phi, q) \left( \gamma_n Jo_n(z, q) + \delta_n No_n(z, q) \right), \quad (\text{B10})$$

where constants  $\alpha_n, \beta_n, \gamma_n, \delta_n$  depend on the boundary conditions. In addition to the external boundary conditions, additional attention should be paid to the segment  $(-a, a)$  corresponding to  $z = 0$ : ordinarily the solutions and their derivatives are continuous across the segment providing a restriction on the coefficients  $\alpha_n \dots \delta_n$ . We,

however, will be also interested in solutions that experience discontinuity across the line, which will provide a different set of constraints on the coefficients in (B10).

c. *Model Schrödinger problem: a particle inside an elliptic box*

We begin with the wave equation describing a particle inside an impenetrable box of elliptical shape. The wavefunction  $\psi$  is assumed to be continuous everywhere inside the ellipse, together with its first derivatives.

It is easy to see that the four products in (B10) and their normal derivatives have the following continuity properties across the segment  $(-a, a)$ :

$F$	$F$ continuous?	$\partial_n F$ continuous?
$ce_n(\phi, q)Je_n(z, q)$	Yes	Yes
$se_n(\phi, q)Jo_n(z, q)$	Yes	Yes
$ce_n(\phi, q)Ne_n(z, q)$	Yes	No
$se_n(\phi, q)No_n(z, q)$	No	Yes

For a particle-in-the-box problem, therefore, the solution must be of the form

$$f = \sum_{n=0} \alpha_n ce_n(\phi, q) Je_n(z, q) + \sum_{n=1} \gamma_n se_n(\phi, q) Jo_n(z, q).$$

Coefficients  $\alpha_n$  and  $\gamma_n$  are determined by the boundary conditions imposed on the exterior boundary of the system. If the boundary of the ellipse is described by  $z = R$ , then the eigenstates can be labelled by two integer indices: the angular index  $n$ , the radial index  $j$ , and their parity under  $\phi \rightarrow -\phi$ . More explicitly, the eigenfunctions are (up to normalization factors)

$$\psi_{nj}^{(e)}(\phi, z) = ce_n(\phi, q_{nj}^e) Je_n(\phi, q_{nj}^e), \quad (\text{B11})$$

$$\psi_{nj}^{(o)}(\phi, z) = se_n(\phi, q_{nj}^o) Jo_n(\phi, q_{nj}^o), \quad (\text{B12})$$

where  $q_{nj}^e$  (or  $q_{nj}^o$ ) is defined as the  $j$ -th solution of  $Je_n(R, q) = 0$  (or  $Jo_n(R, q) = 0$ ). The corresponding energy eigenvalues are

$$E_{nj}^{o(e)} = \frac{\hbar^2}{2m} k^2 = \frac{\hbar^2}{2m} \frac{4q_{nj}^{o(e)}}{a^2}. \quad (\text{B13})$$

## 2. Schrödinger particle in the field of two Aharonov-Bohm half-fluxes

### a. Boundary condition on a segment $z = 0$

To solve the Schrödinger equation

$$(-i\nabla - eA)^2 \psi + k^2 \psi = 0 \quad (\text{B14})$$

with the vector potential  $A(\mathbf{r})$  describing two Aharonov-Bohm fluxes at positions  $(a, 0)$  and  $(-a, 0)$ , we perform

singular gauge transformation

$$\psi \rightarrow f \exp \left( ie \int_{\mathbf{r}_0}^{\mathbf{r}} \mathbf{A}(\mathbf{r}) \cdot d\mathbf{r} \right) . \quad (\text{B15})$$

Since the integral in the exponent depends on the path of integration, we need to introduce a branch cut in order to obtain single-valued functions. We chose the segment  $(-a, a)$  of the real axis as the branch cut:

$$\psi \rightarrow f \exp \left( \frac{i\theta_1 + i\theta_2}{2} \right) , \quad (\text{B16})$$

where  $-\pi \leq \theta_1 < \pi$  and  $0 \leq \theta_2 < 2\pi$ . This transformation eliminates the vector potential, and the resulting equation is just the Helmholtz equation

$$\nabla^2 f + k^2 f = 0 ,$$

except that the solutions must have a branch cut on a segment  $(-a, a)$ :

$$f(x, y + \epsilon) = -f(x, y - \epsilon) \text{ for } x \in (-a, a) .$$

Elliptic coordinates provide a natural framework for imposing the boundary condition:

$$f(z = 0, \phi) = -f(z = 0, -\phi) ,$$

i.e. at  $z = 0$  the solution  $f(z = 0, \phi)$  must be an odd function of  $\phi$ .

Starting from a general form

$$f = \sum_{n=0} ce_n(\phi) [\alpha_n Je_n(z) + \beta_n Ne_n(z)] + \sum_{n=1} se_n(\phi) [\gamma_n Jo_n(z) + \delta_n No_n(z)] , \quad (\text{B17})$$

we obtain for  $f(z = 0, \phi)$ :

$$\sum_{n=0} ce_n(\phi) [\alpha_n Je_n(0) + \beta_n Ne_n(0)] + \sum_{n=1} \delta_n se_n(\phi) No_n(0) ,$$

which implies the following relation between  $\alpha_n$  and  $\beta_n$ :

$$\alpha_n Je_n(0) + \beta_n Ne_n(0) = 0 . \quad (\text{B18})$$

Similarly, the requirement for  $\psi(x, y)$  to have continuous normal derivative across the branch cut yields

$$\frac{\partial}{\partial z} f(z, \phi) |_{z=0} = \frac{\partial}{\partial z} f(z, -\phi) |_{z=0} .$$

Since  $\frac{\partial}{\partial z} f(z, \phi)$  at  $z = 0$  equals

$$\sum_{n=0} ce_n(\phi) [\alpha_n Je'_n(0) + \beta_n Ne'_n(0)] + \sum_{n=1} se_n(\phi) [\gamma_n Jo'_n(0) + \delta_n No'_n(0)] , \quad (\text{B19})$$

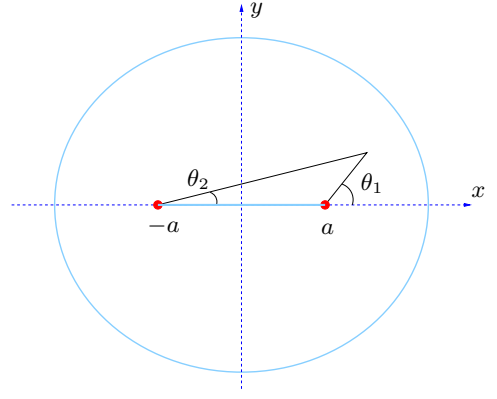


FIG. 12: Two half-fluxes inside an elliptical box.

we obtain

$$\gamma_n Jo'_n(0) + \delta_n No'_n(0) = 0 . \quad (\text{B20})$$

Equations (B18) and (B20) express the continuity of the wavefunction  $\psi(x, y)$  and its normal derivative at the segment  $(-a, a)$ . As a result, the general expression for the wave function has the form

$$f(z, \phi) = \sum_{n=0} \alpha_n(q) ce_n(\phi, q) Le_n(z, q) + \sum_{n=1} \gamma_n(q) se_n(\phi, q) Lo_n(z, q) . \quad (\text{B21})$$

To compactify the notation, we have introduced the following functions:

$$Le_n(z, q) = \frac{Je_n(z, q)}{Je_n(0, q)} - \frac{Ne_n(z, q)}{Ne_n(0, q)} , \quad (\text{B22})$$

$$Lo_n(z, q) = \frac{Jo_n(z, q)}{Jo_n(0, q)} - \frac{No_n(z, q)}{No_n(0, q)} . \quad (\text{B23})$$

At this point one can pose and solve several problems with various external boundary conditions, which we will consider next.

#### b. Schrödinger particle in an elliptical box in the presence of two half-fluxes.

The wavefunctions are zero on the boundary of the elliptical box  $z = R$ , and therefore

$$\sum_{n=0} \alpha_n(q) ce_n(\phi, q) Le_n(R, q) + \sum_{n=1} \gamma_n(q) se_n(\phi, q) Lo_n(R, q) = 0 . \quad (\text{B24})$$

Using orthogonality of  $ce_n(\phi)$  and  $se_n(\phi)$ , we find that the eigenstates of are either even (labeled as “e”) or odd (labeled as “o”) functions of  $\phi$ , and their explicit form,



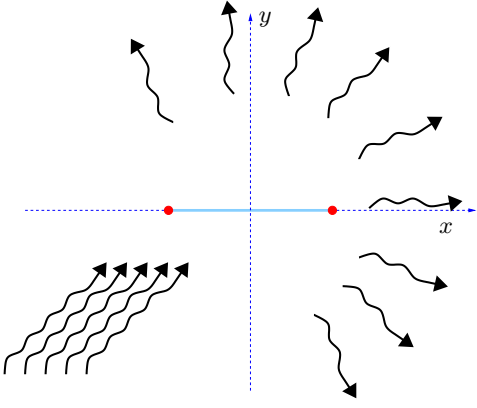


FIG. 13: Two half-fluxes: scattering problem.

up to normalization factors, is given by

$$f_{nj}^{(e)}(z, \phi) = ce_n(\phi, q_{nj}^e) Le_n(z, q_{nj}^e) , \quad (\text{B25})$$

$$f_{nj}^{(o)}(z, \phi) = se_n(\phi, q_{nj}^o) Lo_n(z, q_{nj}^o) , \quad (\text{B26})$$

where  $q_{nj}^e$  and  $q_{nj}^o$  are  $j$ -th solutions of

$$\frac{Je_n(R, q)}{Je_n(0, q)} - \frac{Ne_n(R, q)}{Ne_n(0, q)} = 0 , \quad (\text{B27})$$

$$\frac{Jo_n(R, q)}{Jo_n(0, q)} - \frac{No_n(R, q)}{No_n(0, q)} = 0 \quad (\text{B28})$$

respectively. Therefore, just as in the case of the no-flux problem of the previous section, the eigenstates are classified according to parity under  $\phi \rightarrow -\phi$ , and two integers  $(j, n)$ , where  $j = 1, 2, 3, \dots$ , and  $n = (0), 1, 2, \dots$  for even (odd) solutions. The energy of the eigenstates  $|n, j, o(e)\rangle$  is

$$E_{nj}^{o(e)} = \frac{\hbar^2}{2m} k^2 = \frac{\hbar^2}{2m} \frac{4q_{nj}^{o(e)}}{a^2} . \quad (\text{B29})$$

### c. Scattering of a Schrödinger particle by two fluxes

Now we consider the problem of a particle scattered by two fluxes  $\phi_0/2$  and  $-\phi_0/2$ . To find the scattering cross-section  $\sigma(\hat{\mathbf{n}}, \hat{\mathbf{n}}')$  and the scattering amplitude  $F(\hat{\mathbf{n}}, \hat{\mathbf{n}}')$  we need to match general solution  $f(z, \phi; q)$  given by (B21) with the boundary conditions at infinity that contains only the incoming and the scattered waves:

$$f_{\hat{\mathbf{n}}} = e^{i\mathbf{k}\cdot\mathbf{r}} + \frac{\exp(ikr)}{\sqrt{r}} F(\hat{\mathbf{n}}, \hat{\mathbf{n}}') . \quad (\text{B30})$$

Here,  $\hat{\mathbf{n}} = (\cos\theta, \sin\theta)$  specifies the direction of the incident wave and  $\hat{\mathbf{n}}' = (\cos\phi, \sin\phi)$  describes the direction of scattered wave. The first condition, Eq. (B21), encodes the information about the presence of two half-fluxes, while the second condition, Eq. (B30), restricts

the the wavefunctions to the sum of the incident plane wave  $\exp(i\mathbf{k}\cdot\mathbf{r})$  and the outgoing wave described by the second term. Together, they allow to determine the scattering amplitude unambiguously. To match the two expressions, we write (B30) in terms of Mathieu functions. Expansion of a plane wave  $e^{i\mathbf{k}\cdot\mathbf{r}}$  in Mathieu functions basis has the following form:

$$e^{ik(x \cos\theta + y \sin\theta)} = \sum_{n=0} \rho_n(q) Ce_n(z) ce_n(\phi) ce_n(\theta) + \sum_{n=1} \sigma_n(q) Se_n(z) se_n(\phi) se_n(\theta) , \quad (\text{B31})$$

where the coefficients  $\rho_n(q), \sigma_n(q)$  are related to the known standard factors  $p_n(q), s_n(q)$  from the theory of Mathieu functions (cf. Table V) as

$$\rho_{2n} = \frac{1}{p_{2n}} , \quad \rho_{2n+1} = \frac{i}{p_{2n+1}} , \quad (\text{B32})$$

$$\sigma_{2n} = \frac{1}{s_{2n}} , \quad \sigma_{2n+1} = \frac{i}{s_{2n+1}} . \quad (\text{B33})$$

Now we turn to the scattered wave: the most general expression for the solution, which contains only the outgoing wave, is given by

$$\frac{e^{ikr}}{\sqrt{r}} F(\hat{\mathbf{n}}, \hat{\mathbf{n}}') = \sum_{n=0} \lambda_n ce_n(\phi) ce_n(\theta) He_n^{(1)}(z) + \sum_{n=1} \mu_n se_n(\phi) se_n(\theta) Ho_n^{(1)}(z) . \quad (\text{B34})$$

Functions  $He_n^{(1)}(z)$  and  $Ho_n^{(1)}(z)$ , which play the role of the Hankel functions in the theory of Mathieu equation, are defined as

$$\begin{cases} He_n^{(1)}(z) = Je_n(z) + iNe_n(z) , \\ Ho_n^{(1)}(z) = Jo_n(z) + iNo_n(z) . \end{cases} \quad (\text{B35})$$

Combining (B21), (B31) and B34 we find

$$\lambda_n = -\frac{Je_n(0, q)}{Je_n(0, q) + iNe_n(0, q)} \rho_n , \quad (\text{B36})$$

$$\mu_n = -\frac{Jo_n'(0, q)}{Jo_n'(0, q) + iNo_n'(0, q)} \sigma_n . \quad (\text{B37})$$

We remind the reader that all quantities on the right hand side of (B37) are known, and to obtain the scattering amplitude  $F(\hat{\mathbf{n}}, \hat{\mathbf{n}}')$  from (B34) we only need to use the long distance expressions for  $He_n$  and  $Ho_n$  that are easy to find from Table V:

$$\rho_n He_n \approx \sigma_n Ho_n \approx \left(\frac{4}{\pi^2 q}\right)^{1/4} e^{-z/2 + i\sqrt{q}e^z - i\pi/4} .$$

At large distances, we have  $e^z = 2r/a$ , the elliptic coordinate  $\phi$  is reduced to the ordinary polar angle, and therefore

$$\rho_n He_n \approx \sigma_n Ho_n \approx \left(\frac{a^2}{\pi^2 q}\right)^{1/4} e^{-i\pi/4} \frac{1}{\sqrt{r}} e^{ikr} . \quad (\text{B38})$$

Finally, substitution of these expressions into (B34) yields the following exact expression for the scattering amplitude:

$$F(\theta, \phi) = - \left( \frac{a^2}{\pi^2 q} \right)^{1/4} e^{-i\pi/4} \times \left( \sum_{n=0} \frac{J e_n(0, q)}{H e_n(0, q)} c e_n(\phi, q) c e_n(\theta, q) + \sum_{n=1} \frac{J o'_n(0, q)}{H o'_n(0, q)} s e_n(\phi, q) s e_n(\theta, q) \right). \quad (\text{B39})$$

### 3. Dirac equation

#### a. Relation between Schrödinger and Dirac problems

Now we apply the technique we developed in this appendix to the problem of a Dirac particle moving in the field of two half-fluxes, without specifying the external boundary condition at this point. The Hamiltonian  $H_0$  describing such a system is

$$\begin{pmatrix} 0 & (p_x - eA_x) - i(p_y - eA_y) \\ (p_x - eA_x) + i(p_y - eA_y) & 0 \end{pmatrix},$$

where  $(p_x, p_y)$  is the momentum operator and  $\mathbf{A}$  is the vector potential of the two half-fluxes. Just as for the Schrödinger problem, we perform a unitary transformation (B16), which eliminates the vector potential from the Hamiltonian, but at the expense of introducing a branch cut. After choosing a segment of the real axis  $(-a, a)$  as the location of the branch cut, the eigenfunctions of the Hamiltonian

$$H = e \begin{pmatrix} 0 & p_x - ip_y \\ p_x + ip_y & 0 \end{pmatrix}$$

can be found from the eigenfunctions of the Schrödinger problem, which we described in the previous section: note that if  $f = (u, v)^T$  is an eigenfunction of  $H$ , then it is also an eigenfunction of

$$H^2 = \begin{pmatrix} p_x^2 + p_y^2 & 0 \\ 0 & p_x^2 + p_y^2 \end{pmatrix}.$$

Thus, both  $u$  and  $v$  are solutions of the wave equation

$$(\nabla^2 + E^2)u = 0, \quad (\text{B40})$$

and any solutions of our eigenvalue problem

$$(p_x - ip_y)v = Eu, \quad (\text{B41})$$

$$(p_x + ip_y)u = Ev \quad (\text{B42})$$

can be written as

$$f = \begin{pmatrix} u(x, y) \\ \frac{1}{E}(p_x + ip_y)u(x, y) \end{pmatrix}, \quad (\text{B43})$$

where  $u(\mathbf{r})$  is a solution of (B40). The opposite statement is also clearly valid: for any  $u$ , which satisfies (B40), wavefunction (B43) is an eigenfunction of Hamiltonian  $H$  with energy  $E$ . Thus, it naively appears that all solutions of the Dirac equation can be written as (B43). We will return to the validity of this statement in a moment, but let us first apply (B43) to a simpler problem of a *single-flux* problem.

#### b. The single-flux problem

A problem of *Schrödinger* particle moving in the field of a single half-flux located at the origin is most conveniently solved by eliminating the vector potential by means of  $\psi(\mathbf{r}) = \exp(i\theta/2)f(\mathbf{r})$  transformation, where  $\theta$  is the polar angle. The resulting eigenvalue problem

$$(\nabla^2 + E^2)f = 0 \quad (\text{B44})$$

must be solved in a space of wavefunctions  $f(r, \theta)$  that have a branch-cut extending from 0 to infinity. The cut can be chosen arbitrarily, e.g., as a straight line  $(0, +\infty)$ , or  $(-\infty, 0)$ . The solutions are easily obtained in polar coordinates as

$$f = \sum_{-\infty}^{+\infty} e^{i(m+1/2)\theta} \left[ c_m J_{m+1/2}(kr) + d_m J_{-m-1/2}(kr) \right]. \quad (\text{B45})$$

Consider now a class of problems where the boundary conditions allow the particles to reach the origin – this excludes problems where impenetrable walls of finite radius surround the flux.

The requirement of square-integrability of the wavefunctions requires that all coefficients  $d_m, m \geq 0$  and  $c_m, m < 0$  must be set to zero except, possibly,  $d_0$  and  $c_{-1}$ . The eigenfunctions corresponding to  $c_{-1}$  and  $d_0$  are divergent at the origin, but square integrable. Ordinarily, physical realization of the flux requires the wavefunctions to be not only square-integrable, but also finite at  $r = 0$ : this eliminates the remaining arbitrariness and results in  $d_m = 0$  for all  $m \geq 0$ , and  $c_m = 0$  for all  $m < 0$ . Thus, for every angular channel  $m$  there is only one radial solution:

$$\psi = e^{i\theta/2} f = \sum_{-\infty}^{+\infty} a_m e^{im\theta} J_{|m-1/2|}(Er),$$

however, (B44) is used as an auxiliary tool to obtain solutions of the Dirac problem via Eq. (B43), requirement of the wavefunctions being finite at  $r = 0$  is too restrictive: even if the upper components  $u$  of solutions are chosen to be finite, then the lower component of at least some wavefunctions will necessarily be divergent, but square integrable at the origin. To consider the most general situation, however, we choose  $u$  is the form of (B45) allowing at this stage all square integrable wavefunctions. Using (B43) and the following expressions:

$$\partial_x \pm i\partial_y = e^{\pm i\theta} \left( \partial_r \pm \frac{i}{r} \partial_\theta \right), \quad (\text{B46})$$

the solutions of the Dirac equation can be written as

$$f = \sum_m e^{i(m+\frac{1}{2})\theta} (c_m \chi_m^{(+)} + d_m \chi_m^{(-)}),$$

where

$$\chi_m^{(\pm)} = \begin{pmatrix} J_{\pm(m+\frac{1}{2})}(Er) \\ -ie^{i\theta} \left[ J'_{\pm(m+\frac{1}{2})}(Er) - \frac{(m+\frac{1}{2})}{Er} J_{\pm(m+\frac{1}{2})}(Er) \right] \end{pmatrix}. \quad (\text{B47})$$

Using the standard identities for Bessel functions,  $f$  can be written as

$$f = \sum_m e^{i(m+\frac{1}{2})\theta} \left[ c_m \begin{pmatrix} J_{m+\frac{1}{2}}(Er) \\ ie^{i\theta} J_{m+\frac{3}{2}}(Er) \end{pmatrix} + d_m \begin{pmatrix} J_{-m-\frac{1}{2}}(Er) \\ -ie^{i\theta} J_{-m-\frac{3}{2}}(Er) \end{pmatrix} \right] \quad (\text{B48})$$

For all values of  $m \geq 0$  ( $m \leq -2$ ) the requirement of square-integrability demands that  $d_m = 0$  ( $c_m = 0$ ). At  $m = -1$ , however there is an ambiguity. It is impossible *a priori* to decide which of the two radial functions

$$\begin{pmatrix} J_{-\frac{1}{2}}(Er) \\ ie^{i\theta} J_{\frac{1}{2}}(Er) \end{pmatrix} \text{ or } \begin{pmatrix} J_{\frac{1}{2}}(Er) \\ -ie^{i\theta} J_{-\frac{1}{2}}(Er) \end{pmatrix} \quad (\text{B49})$$

should be used. Either the upper or the lower component of the wavefunction is divergent, but still square integrable. The attempt to set both  $c_{-1}$  and  $d_{-1}$  to zero leads to the loss of completeness in the angular basis: the wavefunctions described by  $f \propto \exp(-i\theta/2)$  or, equivalently, the original gauge wavefunctions  $\psi$  which do not have angular dependence, would be left out of the Hilbert space. On the other hand, to require that both solutions are present in the spectrum independently would be too much: the resulting set of basis functions is then overcomplete. As was shown by Jackiw and Gerbert, the solution is to use one linear combination of the two solutions. Different regularizations of the problem then correspond to different choice of the linear combination. Importantly, not all linear combinations are mathematically allowed, and can emerge from the regularized problems: the relative phase of  $c_{-1}$  and  $d_{-1}$  turns out to be fixed, and different boundary conditions, forming different self-adjoint extensions of the problem are described through a single parameter  $\theta$ . For a given  $\theta$  the divergent part of the wavefunctions is

$$\frac{1}{\sqrt{r}} \begin{pmatrix} \sin \theta \\ -ie^{i\phi} \cos \theta \end{pmatrix}. \quad (\text{B50})$$

Note that in this problem the basis functions have a useful property: both the upper component and the lower component can be simultaneously written as separable functions, i.e. a product of two functions that depend only on  $\theta$  and only on  $r$ . This is a peculiarity of the single-flux problem, and in general this property does not

hold. Nevertheless, although the analysis will be slightly more complicated, all essential properties of the single-flux problem such as the necessity of additional boundary conditions at flux locations and the form of the boundary conditions remain valid in the case of two-flux problem as well.

### c. Dirac particle in the presence of two half-fluxes

Once again, we use (B43) to construct solutions of Dirac equation from the solutions (B21) of the wave equation in the presence of two half-fluxes. In elliptical coordinates,

$$\partial_x + i\partial_y = \frac{1}{a \sinh z \cos \phi - a \cosh z \sin \phi} (\partial_z + i\partial_\phi).$$

The eigenfunctions of the Dirac equation obtained from (B43) and (B21) can be written now as

$$\sum_{n=0} \alpha_n(q) \chi_n^{(+)} + \sum_{n=1} \beta_n(q) \chi_n^{(-)}, \quad (\text{B51})$$

where spinors  $\chi_n^{(\pm)}$  are equal to

$$\chi_n^{(+)} = \begin{pmatrix} ce_n(\phi) Le_n(z, q) \\ -\frac{i}{E} \frac{ce_n(\phi) Le'_n(z) + i ce'_n(\phi) Le_n(z)}{a \sinh z \cos \phi - a \cosh z \sin \phi} \end{pmatrix}. \quad (\text{B52})$$

and

$$\chi_n^{(-)} = \begin{pmatrix} se_n(\phi) Lo_n(z, q) \\ -\frac{i}{E} \frac{se_n(\phi) Lo'_n(z) + i se'_n(\phi) Lo_n(z)}{a \sinh z \cos \phi - a \cosh z \sin \phi} \end{pmatrix}. \quad (\text{B53})$$

So far we almost literally followed the route of the single half-flux problem. However, even a cursory examination of the solutions  $\chi_n^{(\pm)}$  shows that something is amiss. In obtaining (B21) and then  $\chi_n^{(\pm)}$ , we never discarded any solutions, and yet the upper components of all  $\chi_n^{(\pm)}$  are always perfectly regular. So, where are the wavefunctions with upper components divergent near the half-fluxes?

Before we answer this question, let us examine the lower components of the solutions. The elliptical coordinates of the flux located at  $(x, y) = (a, 0)$  are  $(z, \phi) = (0, 0)$ . Therefore, in the vicinity of this flux, we have

$$\frac{1}{a \sinh z \cos \phi - a \cosh z \sin \phi} \approx \frac{1}{a(z - i\phi)} \approx \frac{e^{i\theta_1/2}}{\sqrt{2a\rho_1}}, \quad (\text{B54})$$

where  $\rho_1$  is the distance between the point  $(x, y)$  and the flux, and  $\theta_1 \in (-\pi, \pi)$  is the polar angle shown in Fig. 12. Similarly, near the second flux at  $(-a, 0)$ , we have  $(z, \phi) \approx (0, \pi)$ , and therefore

$$\frac{1}{a \sinh z \cos \phi - a \cosh z \sin \phi} \approx \frac{1}{a(z - i\phi)} \approx \frac{e^{i\theta_2/2 - i\pi/2}}{\sqrt{2a\rho_2}}.$$

Since  $Le_n(z=0, q) = 0$  and  $Lo'_n(z=0, q) = 0$ , in the vicinity of the first flux, the divergent part of  $\chi_n^{(\pm)}$  is

$$\chi_n^{(+)} = -\frac{ic e_n(0, q) Le'_n(0, q)}{E} \frac{e^{i\theta_1/2}}{\sqrt{2a\rho_1}} \begin{pmatrix} 0 \\ 1 \end{pmatrix}, \quad (\text{B55})$$

$$\chi_n^{(-)} = \frac{se'_n(0, q) Lo_n(0, q)}{E} \frac{e^{i\theta_1/2}}{\sqrt{2a\rho_1}} \begin{pmatrix} 0 \\ 1 \end{pmatrix}. \quad (\text{B56})$$

The divergent part of the wavefunctions near the second flux is almost identical:

$$\chi_n^{(+)} = -\frac{ic e_n(\pi, q) Le'_n(0, q)}{E} \frac{e^{i\theta_2/2 - i\pi/2}}{\sqrt{2a\rho_2}} \begin{pmatrix} 0 \\ 1 \end{pmatrix}, \quad (\text{B57})$$

$$\chi_n^{(-)} = \frac{se'_n(\pi, q) Lo_n(0, q)}{E} \frac{e^{i\theta_2/2 - i\pi/2}}{\sqrt{2a\rho_2}} \begin{pmatrix} 0 \\ 1 \end{pmatrix}. \quad (\text{B58})$$

Comparison with the single half-flux boundary condition at the flux location (B50) suggests that the wavefunctions  $\chi_n^{\pm}$ , which we just constructed, are merely one of many possible self-adjoint extensions. This extension contains wavefunctions which near both fluxes have regular upper components and divergent lower component.

What about the other self-adjoint extensions? Where did we lose them? After all, we only repeated the steps for the single flux Aharonov-Bohm problem, where this approach allowed us to find all self-adjoint extensions. Why didn't they naturally appear from (B43)?

To understand what went wrong, consider again solutions of the Schrödinger equations for the single half-flux (B45) and compare them to general solution of the Schrödinger solution for the two half-fluxes problem (B21). One glaring distinction is that the former contains solutions divergent near the fluxes, while the latter does not! To be sure, there are certainly solutions of the two-flux problem that diverge near the fluxes – moreover, we constructed them explicitly, when we found the lower components of  $\chi_n^{\pm}$ . The paradox appeared because these divergent solutions do *not* have a separable form  $f_1(z)f_2(\phi)$  because the fluxes are point-like defects. The line connecting the two fluxes, and the elliptical coordinates used to describe it were just tools, which allowed us to analyze the problem analytically, but the underlying structure of the divergencies is still that of point

like defects. They are, naturally, most easily described in local polar coordinate system around each flux. The functional form of the singularities, which has a structure  $F_1(\rho_i)F_2(\theta_i)$ , is incompatible with a factorization  $f_1(z)f_2(\phi)$ , as can be seen for example from (B54).

In short, we were able to find the self-adjoint extension Eq. (B51)-(B53) analytically in elliptical coordinates so easily only because we started with the regular upper components. Then it was easy to construct a complete basis of wavefunctions of the form  $ce_n(\phi)Le_n(z)$  and  $se_n(\phi)Lo_n(z)$ . Only then we worked out the lower components, which ended up divergent near flux locations, but not factorizable.

Can we find other self-adjoint extensions using elliptical coordinates? There is one other case that is easy to solve: wavefunctions with the regular lower component. Rather than using (B43), we could have tried the form

$$f = \begin{pmatrix} \frac{1}{E}(p_x - ip_y)v(x, y) \\ v(x, y) \end{pmatrix}. \quad (\text{B59})$$

We would start from the regular solutions of the wave equation for  $v$ :

$$v(\phi, z) = \sum \alpha_n ce_n(\phi)Le_n(z) + \beta_n se_n(\phi)Lo_n(z),$$

and then would apply operator  $(p_x - ip_y)/E$  to find the upper components of the spinors forming the basis. This naturally would result in a self-adjoint extension with the regular lower components, and divergent upper components – the opposite of the first self-adjoint extension we found in (B51-B53). Note that these two self-adjoint extensions just found, with the regular upper or lower components, are the ones that follow from the simplest physical regularizations<sup>64</sup> of the problem obtained by replacing each of the the infinitely thin Aharonov-Bohm strings by a solenoid of finite radius.

Can one do better and construct the basis analytically for the general case, with arbitrary parameters  $\theta_{1,2}$  characterizing via (B50) each of the fluxes? At present, we do not know the answer to this question, and leave this interesting problem for future study.

\* Electronic address: ashot@phys.ufl.edu

† Electronic address: zbt@pha.jhu.edu

<sup>1</sup> C. Caroli, P. G. deGennes, and J. Matricon, Phys. Lett. **9**, 307 (1964).

<sup>2</sup> M. Franz and Z. Tešanović, Phys. Rev. Lett. **80**, 4763 (1998).

<sup>3</sup> Of course, some of the low energy states are strongly peaked near a vortex. Even such states, however, do “leak out” into the continuum and develop power law decay, mostly along nodal directions.

<sup>4</sup> G. E. Volovik, JETP Lett. **58**, 469 (1993). For a detailed critique of a Doppler shift method within the context of the full quasiclassical approach see T. Dahm, S. Graser, C. Iniotakis, and N. Schopohl, Phys. Rev. B **66**, 144515 (2002).

<sup>5</sup> K. Yasui and T. Kita, Phys. Rev. Lett. **83**, 4168 (1999); K. Yasui and T. Kita, Phys. Rev. B **66**, 184516 (2002).

<sup>6</sup> Y. Wang and A. H. MacDonald, Phys. Rev. B **52**, R3876 (1995).

<sup>7</sup> S. H. Simon and P. A. Lee, Phys. Rev. Lett. **78**, 1548

- (1997).
- <sup>8</sup> M. Franz and Z. Tešanović, Phys. Rev. Lett. **84**, 554 (2000).
  - <sup>9</sup> L. Marinelli, B. I. Halperin, and S. H. Simon, Phys. Rev. B **62**, 3488 (2000); L. Marinelli and B. I. Halperin, *ibid.* **65**, 014516 (2002).
  - <sup>10</sup> O. Vafek, A. Melikyan, M. Franz, and Z. Tešanović, Phys. Rev. B **63**, 134509 (2001); O. Vafek, A. Melikyan, and Z. Tešanović, *ibid.* **64**, 224508 (2001).
  - <sup>11</sup> A. Vishwanath, Phys. Rev. Lett. **87**, 217004 (2001).
  - <sup>12</sup> A. Vishwanath, Phys. Rev. B **66**, 064504 (2002).
  - <sup>13</sup> D. Knapp, C. Kallin, and A. J. Berlinsky, Phys. Rev. B **64**, 014502 (2001); D. Knapp, C. Kallin, A. J. Berlinsky, and R. Wortis, *ibid.* **66**, 144508 (2002).
  - <sup>14</sup> J. Goryo and M. Kohmoto, Phys. Rev. B **66**, 174503 (2002).
  - <sup>15</sup> M. Franz and Z. Tešanović, Phys. Rev. Lett. **87**, 257003 (2001); Z. Tešanović, O. Vafek, and M. Franz, Phys. Rev. B **65**, 180511 (2002).
  - <sup>16</sup> I. F. Herbut, Phys. Rev. Lett. **88**, 047006 (2002).
  - <sup>17</sup> J. Ye, Phys. Rev. Lett. **86**, 316 (2001).
  - <sup>18</sup> D. V. Khveshchenko and A. G. Yashenkin, Phys. Rev. B **67**, 052502 (2003); Phys. Lett. **A309**, 363 (2003).
  - <sup>19</sup> J. Lages, P. D. Sacramento, and Z. Tešanović, Phys. Rev. B **69**, 094503 (2004).
  - <sup>20</sup> J. Lages and P. D. Sacramento, Phys. Rev. B **71**, 132501 (2005).
  - <sup>21</sup> P. Nikolic and S. Sachdev, cond-mat/0511298.
  - <sup>22</sup> The reader will realize that the linearized approximation discussed here is valid only sufficiently far from vortex cores. For many purposes, however, this is precisely what is needed since the thermodynamics and quasiparticle transport at low fields ( $l \gg \xi$ ) are dominated by properties of nodal quasiparticles in the bulk, far away from vortex locations. The effective theory corresponding to this linearized version of the BdG problem generally exhibits characteristic universal scaling of quasiparticle thermodynamics and transport properties, the dimensionless scaling parameter being the ratio of thermal to magnetic length<sup>7</sup>. The actual form of various scaling functions and quasiparticle energy spectrum follow directly from the approach of FT<sup>8</sup>.
  - <sup>23</sup> B. W. Hoogenboom, K. Kadowaki, B. Revaz, M. Li, Ch. Renner, and Ø. Fischer, cond-mat/0105528; I. Maggio-Aprile, Ch. Renner, A. Erb, E. Walker, and Ø. Fischer, Phys. Rev. Lett. **75**, 2754 (1995); Ch. Renner, B. Revaz, K. Kadowaki, I. Maggio-Aprile, and Ø. Fischer, *ibid.* **80**, 3606 (1997); B. W. Hoogenboom, Ch. Renner, B. Revaz, I. Maggio-Aprile, and Ø. Fischer, Physica C, **332**, 440 (2000).
  - <sup>24</sup> D. P. Arovas, A. J. Berlinsky, C. Kallin, and S.-C. Zhang, Phys. Rev. Lett. **79**, 2871 (1997).
  - <sup>25</sup> B. M. Andersen, H. Bruus, and P. Hedegård, Phys. Rev. B **61**, 6298 (2000).
  - <sup>26</sup> M. Franz and Z. Tešanović, Phys. Rev. B **63**, 064516 (2001).
  - <sup>27</sup> J. H. Han and D.-H. Lee, Phys. Rev. Lett. **85**, 1100 (2000).
  - <sup>28</sup> E. Demler, S. Sachdev, and Y. Zhang, Phys. Rev. Lett. **87**, 067202 (2001).
  - <sup>29</sup> Q.-H. Wang, J. H. Han, D.-H. Lee, Phys. Rev. Lett. **87**, 167004 (2001).
  - <sup>30</sup> J.-X. Zhu and C. S. Ting, Phys. Rev. Lett. **87**, 147002 (2001).
  - <sup>31</sup> C. Berthod and B. Giovannini, Phys. Rev. Lett. **87**, 277002 (2001).
  - <sup>32</sup> M. Franz, D. E. Sheehy and Z. Tešanović, Phys. Rev. Lett. **88**, 257005 (2002).
  - <sup>33</sup> J.-X. Zhu, C. S. Ting, and A. V. Balatsky, Phys. Rev. B **66**, 064509 (2002).
  - <sup>34</sup> X. Yang and C. Nayak, Phys. Rev. B **65**, 064523 (2002).
  - <sup>35</sup> H. K. Nguyen and S. Chakravarty, Phys. Rev. B **65**, 180519 (2002).
  - <sup>36</sup> J.-X. Zhu, I. Martin, and A. R. Bishop, Phys. Rev. Lett. **89**, 067003 (2002).
  - <sup>37</sup> J. Kishine, P. A. Lee, and X.-G. Wen, Phys. Rev. B **65**, 064526 (2002).
  - <sup>38</sup> L. B. Ioffe and A. J. Millis, Phys. Rev. B **66**, 094513 (2002).
  - <sup>39</sup> A. Ghosal and C. Kallin and A. J. Berlinsky, Phys. Rev. B **66**, 214502 (2002).
  - <sup>40</sup> H. Tsuchiura, M. Ogata, Y. Tanaka, and S. Kashiwaya, Phys. Rev. B **68**, 012509 (2003).
  - <sup>41</sup> For a comprehensive review of Dirac fermions in the context of (disordered) superconductors see A. Altland, B. D. Simons, and M. R. Zirnbauer, Phys. Rep. **359**, 283 (2002).
  - <sup>42</sup> The low energy physics of nodal quasiparticles is fully specified by two (suitably renormalized) velocities,  $v_F$  and  $v_\Delta$ : A. C. Durst and P. A. Lee, Phys. Rev. B **62**, 1270 (2000). The experimental confirmation of this and direct measurements of the  $v_\Delta/v_F$  ratio from thermal conductivity are found in Ref. 43.
  - <sup>43</sup> M. Chiao, R. W. Hill, C. Lupien, L. Taillefer, P. Lambert, R. Gagnon, and P. Fournier, Phys. Rev. B **62**, 3554 (2000); D. G. Hawthorn, S. Y. Li, M. Sutherland, Etienne Boaknin, R. W. Hill, C. Proust, F. Ronning, M. A. Tanatar, Johnpierre Paglione, D. Peets, Ruixing Liang, D. A. Bonn, W. N. Hardy, N. N. Kolesnikov, and L. Taillefer, cond-mat/0502273.
  - <sup>44</sup> B. Lake, G. Aeppli, K. N. Clausen, D. F. McMorrow, K. Lefmann, N. E. Hussey, N. Mangkorntong, M. Nohara, H. Takagi, T. E. Mason, and A. Schröder, Science **291**, 1759 (2001).
  - <sup>45</sup> Throughout the paper we assume that  $k_F^{-1}$  is smaller than but still roughly comparable to  $\xi$  since this is the case for cuprate superconductors. Both lengths are far shorter than magnetic length  $l$  in the low-field regime discussed here ( $l \gg \xi \gtrsim k_F^{-1}$ ).
  - <sup>46</sup> In a separate companion paper<sup>47</sup>, we show through a detailed analysis of numerical solutions of the *lattice*  $d$ -wave superconductor at various magnetic fields that the low magnetic field limit is *non-uniform*, in the sense that it does not naturally select a single universal self-adjoint extension but instead leads to a family of scaling behaviors determined by the commensuration of the magnetic length and the underlying tight-binding atomic lattice. This “non-universality” is due to the fact the nodes of a  $d$ -wave superconductor are not located at  $k = 0$ , as those of a Dirac equation, but at *finite*  $k = k_F$  and thus a new dimensionless parameter  $k_F a$  (or  $k_F \xi$ ) appears which regulates rapid oscillations of the quasiparticle spectra, even in the  $H \rightarrow 0$  limit.
  - <sup>47</sup> A. Melikyan and Z. Tešanović, unpublished.
  - <sup>48</sup> M. V. Berry and R. J. Mondragon, Proc. R. Soc. London, Ser. A **412**, 53 (1987); P. Alberto, C. Fiolhais, and V. M. S. Gil, Eur. J. Phys. **19**, 553 (1998); P. Alberto, C. Fiolhais, and M. Oliveira, *ibid.* **17**, 19 (1996).
  - <sup>49</sup> Similar difficulties also appear when the problem is tackled in the original Simon-Lee basis, i.e. prior to FT transformation. Since the solutions form representations of magnetic translation group, a magnetic unit cell must first be

- chosen. Again, the choice is not unique: for example, the magnetic unit cell containing two vortices can be selected to be a rectangle  $l \times 2l$  or a square  $\sqrt{2}l \times \sqrt{2}l$  and the density of states in the two cases is different when calculated numerically. It should be stressed that this problem *does not* appear for the BdG equations on a tight-binding lattice<sup>10</sup>, where various singular gauge transformations are exact finite unitary rotations. These difficulties associated with the linearized description have long been anticipated to be a consequence of the singular nature of the perturbations and the necessity of regularizing the problem near vortices<sup>10,12</sup>.
- <sup>50</sup> E. Brown, Phys. Rev. **133**, A1038 (1964).
- <sup>51</sup> J. Zak, Phys. Rev. **134**, A1602 (1964); **134**, A1607 (1964).
- <sup>52</sup> Y. A. Bychkov and E. I. Rashba, Zh. Eksp. Teor. Fiz. **85**, 1826 (1983) [Sov. Phys. JETP **58**, 1062 (1983)].
- <sup>53</sup> S. Dukan, A. V. Andreev and Z. Tešanović, Physica C **183**, 355 (1991); S. Dukan and Z. Tešanović, Phys. Rev. B **49**, 13017 (1994).
- <sup>54</sup> H. Aker, A. H. MacDonald, S. M. Girvin and M. R. Norman, Phys. Rev. Lett. **67**, 2375 (1991); A. H. MacDonald, H. Aker and M. R. Norman, Phys. Rev. B **45**, 10147 (1992).
- <sup>55</sup> An explicit expression for  $\phi_{A(B)}(\mathbf{r})$  in terms of the anti-symmetric elliptic theta function can be found in Ref. 9.
- <sup>56</sup> In the FT gauge a BdG quasiparticle acquires the  $\pm\pi$  geometric phase *gradually* as it moves around a vortex. Such half-flux Aharonov-Bohm effect can be gauge-transformed into a branch cut, emanating at a vortex and extending to infinity, across which the wavefunction *abruptly* switches its sign. This “symmetric” gauge (in parlance of Ref. 8), however, leads to non single-valued wavefunctions and ensuing complications. Since the original BdG problem obviously involves only single-valued quasiparticle wavefunctions, a gradual acquisition of the Berry phase through a half-flux Aharonov-Bohm effect is a more natural gauge choice.
- <sup>57</sup> For two different arbitrary A-B partitions there is no simple relation between the two band structures  $E(\mathbf{k})$ , and only the density of states must be equal. The two choices of A-B sublattices shown in Fig. 2, however, are related by a diagonal *anti-periodic* gauge transformation, and therefore direct comparison of the dispersions can be done. Additionally, we verified that the features of the DOS computed for “AABB” and “ABAB” partitions exhibit qualitative differences, such as the slope of the DOS at zero momentum and the energy values at which van Hove singularities occur.
- <sup>58</sup> Additionally, in situations where there is no underlying lattice, like superfluid  $^3\text{He}$ , we must deal with continuum formulation from the outset (A recent review gives an extensive account of vortex-quasiparticle dynamics in continuum models and contains a useful list of references: N. B. Kopnin, Reports Prog. Phys. **65**, 1633 (2002). However, the reader should be warned that many of the results are obtained within various semiclassical approximations – frequently justified in conventional superconductors and  $^3\text{He}$  on the grounds of  $k_F\xi \gg 1$  – and should be critically reevaluated when applied to high temperature superconductors, particularly in the underdoped regime, where quantum effects are crucial).
- <sup>59</sup> A. S. Mel’nikov, Phys. Rev. Lett. **86**, 4108 (2001).
- <sup>60</sup> Although formally all eigenfunctions of the spectrum diverge near vortices according to (10) or (11), the prefactor of the divergent part of the wavefunctions rapidly decreases as a function of the energy  $|E|$ . Therefore in practice the singular  $r^{-1/2}$  behavior of the wavefunctions describing higher energy bands can be detected only at distance very near a vortex. For sufficiently high energies, such distance becomes comparable to the vortex core size, where the linearization is not valid.
- <sup>61</sup> Ph. de Sousa Gerbert and R. Jackiw, MIT Report No. CTP-1594, 1988 (unpublished); Ph. de Sousa Gerbert, Phys. Rev. D **40**, 1346 (1989).
- <sup>62</sup> The self-adjoint extensions described in the text have the property that near each vortex *all* wavefunctions of the spectrum are described by the same singular asymptotic behavior  $|\mathbf{r} - \mathbf{R}_i|^{-1/2}\psi(\phi_i)$ , where  $\phi_i$  is the polar angle in the coordinate system centered around the position of vortex  $\mathbf{R}_i$  and the angular dependence  $\psi(\phi_i)$  is determined by a single parameter  $\theta_i$ . In general, there are other mathematically legitimate self-adjoint extensions where instead it is certain linear combinations of divergent parts near *different* vortices that are the same for all wavefunctions. In this paper we consider only the extensions of the first class.
- <sup>63</sup> M. Reed and B. Simon, *Fourier Analysis and Self-Adjointness* (Academic, New York 1975).
- <sup>64</sup> M. G. Alford, J. March-Russel, and F. Wilczek, Nucl. Phys. **B328**, 140 (1989).
- <sup>65</sup> A. Melikyan and Z. Tešanović, in preparation.
- <sup>66</sup> M. Tinkham, *Introduction to Superconductivity* (Krieger, Malabar, 1975).
- <sup>67</sup> Operators  $D(g)$  are said to form *ray* representations of group  $G$ , if  $D(g_1)D(g_2) = \alpha(g_1, g_2)D(g_1g_2)$ , where  $\alpha$  is a scalar. For instance, for the group considered in the text  $D(m_x)D(m_y)\Psi = -D(m_y)D(m_x)\Psi$  while the group elements  $m_x$  and  $m_y$  commute:  $m_xm_y = m_y m_x = I$ .
- <sup>68</sup> The points of the BZ with crystal momentum belonging to the symmetry lines  $k_x = -k_x$  and  $k_y = -k_y \pmod{2\pi/l}$  but do not coincide with  $X$ ,  $\Gamma$ ,  $M$  and  $Y$  are invariant under  $Cm_x$  ( $Pm_y$ ), however it is easy to show that the representations of this subgroup are one-dimensional and do not result in degeneracy of the states with such momenta.
- <sup>69</sup> The proof of the degeneracy of the spectrum by Vishwanath<sup>11,12</sup> assumes periodicity of quantity  $\Phi_{\{q\}}^2$ , denoted by  $\exp(-\delta\phi)$  by this author. Actually, this quantity is anti-periodic as shown in the Appendix. Nevertheless, the conclusions regarding the degeneracy of the spectrum at points  $\Gamma$  and  $M$  remain valid as follows from (28).
- <sup>70</sup> O. Vafek and A. Melikyan, Phys. Rev. Lett. **96**, 167005 (2006).
- <sup>71</sup> N. W. McLachlan, *Theory and Applications of Mathieu Functions* (Dover, New York, 1964).
- <sup>72</sup> P. M. Morse and H. Feshbach, *Methods of Theoretical Physics* (McGraw-Hill, New York, 1953).
- <sup>73</sup> M. Abramowitz and I. A. Stegun, *Handbook of Mathematical Functions* (Dover, New York, 1965).